WILEY

| RESEARCH ARTICLE OPEN ACCESS

Wavelet-Based Stochastic Model for the Generation of Fully Nonstationary Bidirectional Seismic Accelerograms

Hera Yanni[1] ⓘ | Michalis Fragiadakis[1] ⓘ | Ioannis P. Mitseas[1,2] ⓘ

[1]School of Civil Engineering, National Technical University of Athens, Athens, Greece | [2]School of Civil Engineering, University of Leeds, Leeds, UK

Correspondence: Michalis Fragiadakis (mfrag@mail.ntua.gr)

ABSTRACT

A new stochastic methodology is proposed for the generation of bidirectional horizontal components of artificial, fully nonstationary, site- and spectrum-compatible seismic accelerograms through a nonseparable process. The model operates in the time-frequency domain and combines spectral representation techniques with signal processing tools. The basis of the methodology involves the generation of spectrum-compatible stationary artificial accelerogram signals whose nonstationarity is then modeled with a time-frequency modulating function that is based on a seed ground motion record. At the core of the proposed methodology lies the use of the Continuous Wavelet Transform (CWT). Specifically, the CWT method is used to perform time-frequency analysis and to define the nonstationary component. The proposed methodology provides any required number of seismic accelerograms whose temporal and spectral modulation is consistent with the characteristics of the site of interest. Furthermore, the model is extended to the case of pairs of bidirectional horizontal components. This is accomplished by probabilistically generating two orthogonal spectra whose geometric mean spectrum is compatible with a target spectrum. This procedure also takes into account the correlation structure of spectral acceleration pairs in orthogonal directions at different periods based on empirical models. The bidirectional components are then generated with the proposed site and spectrum-based methodology. An online tool that implements the proposed methodology is freely provided.

1 | Introduction

The continuous advancements of computational capabilities offer new opportunities for the performance assessment of structural systems under earthquake loading. That is, the time history analysis (THA) method is becoming more and more popular in every-day engineering practice. Moreover, new approaches to structural analysis tend to incorporate probabilistic models that account for uncertainties and variations in ground motions as well as in structural properties [1]. Pertinent models include Monte Carlo simulation (MCS) methods [2] and stochastic dynamics techniques [3–6], as well as intensity measure (IM) approaches

like incremental dynamic analysis, cloud analysis, multiple-stripe analysis methods [7], and surrogate modeling approaches [8].

The input earthquake actions for seismic performance assessment can be either past-recorded ground motions or artificial acceleration time-histories. The MCS-based techniques mostly rely on artificially generated seismic records representing the ground motion, whereas several approaches where the random vibration is of significance rely upon the fundamental concept of the power spectrum as a core model for both excitation and response process representation [3–6]. When THA and IM approaches are adopted, engineers typically resort

to the selection and scaling of past-recorded ground motions obtained from online databases. However, this practice remains a highly controversial issue in the relevant literature, as several studies have demonstrated that record scaling may be a source of bias [9, 10]. Moreover, past-recorded accelerograms inherently correspond to different seismic hazard, site, and soil conditions. Finally, even though the online databases are constantly enriched with new records, there is still a lack of ground motions from earthquakes with large magnitudes at small epicentral distances.

Within this framework, the use of artificial accelerograms is an alternative that effectively overcomes many of the problems associated with the use of natural seismic records. Artificial earthquake ground motions can be designed to feature site-consistent characteristics, as well as compatibility with the seismic hazard scenario of interest. Given the inherently random nature of seismic actions, artificial earthquake ground motions are typically modeled as stochastic processes and fields. The various approaches that have been proposed in the literature range from *source-based models* that follow a seismological approach like the point source modeling [11, 12] and the finite fault modeling [12], to *site-based models* that simulate acceleration time-histories based on seed ground motion records [13–15]. A third option is the *spectrum-based models* that focus on generating artificial accelerograms that are compatible with a target design spectrum [14, 16–22]. It is noted that the most suitable approaches for every-day engineering applications should comply with site and/or spectrum-dictated requirements, thus, *site-based* and *spectrum-based models* are of main interest. More recently, *site-based models* have been expanded to include the modeling of several ground motion parameters based on the regression analysis of recorded ground motions from online databases [23–26]. Furthermore, other recent methodologies adopt machine learning techniques for the generation of artificial waveforms [27].

The aforementioned works focus on the generation of single-component ground motions. Nevertheless, seismic motions are three-dimensional phenomena; therefore, in the context of THA, multi-component acceleration time-histories are required. However, only a limited number of past studies focus on the simulation of multi-component motions, and they typically follow a similar approach, which is based on feature extraction from online databases like the PEER NGA-West 2 database [28]. For example, references [24, 29, 30] extend existing site-based models [13, 23] based on the regression analysis of recorded ground motions from online databases. Studies focusing on the simulation of spatially correlated acceleration time-histories [31] have also been proposed.

The spectral representation method (SRM) [32] employs the theory of stochastic processes and, combined with the evolutionary spectra theory [33], is one of the earliest and most widely adopted approaches for the generation of artificial seismic ground motions. Furthermore, based on the relationship between the values of the power spectral density (PSD) function of the stochastic process and the response spectral values for a given spectral damping ratio [34], time-histories that are compatible with a target code-compliant pseudo-acceleration response spectrum can be generated. The seismic signals generated following the SRM can be stationary [32], quasi-stationary [17], and fully nonstationary. Stationary signals exhibit no amplitude

or frequency variation in time, whereas quasistationary signals achieve only amplitude variation over time with a constant frequency content. Fully nonstationary signals resemble the nature of real seismic ground motions by featuring an evolving amplitude and frequency content in time. The generation of fully nonstationary acceleration time-histories using the SRM is typically based on the evolutionary power spectral density (EPSD) function modeling [18]. Specifically, the EPSD function can be either constructed directly through a mathematical model [25], or by introducing a time-frequency modulating function that modifies the PSD function of a stationary stochastic process [16, 35]. Alternatively, the EPSD function can be modeled by exploiting the nonstationary properties of real recorded ground motions [14].

Recent methodologies for generating fully nonstationary seismic ground motions resort to signal processing operations in order to effectively model the signal's evolving amplitude and frequency content. These techniques find increased interest due to their ability to analyze and synthesize the signals simultaneously in both the time and frequency domain, thus allowing the direct modeling of their nonstationary characteristics. Such approaches involve the use of the Fourier Transform (FT) [22], the S-Transform [26], the Hilbert–Huang Transform [20], and Wavelet Transform (WT) methodologies. The WT is a powerful tool for obtaining a joint time-frequency representation of nonstationary signals. More specifically, it employs localized wave-like functions known as *wavelets* instead of continual harmonics as a base to decompose a signal. Among various WT methodologies for generating artificial ground motions are the wavelet packet transform [23, 30], the Discrete Wavelet Transform [15], the Harmonic Wavelet Transform [21, 36], and the Continuous Wavelet Transform (CWT) [37]. The choice of an appropriate joint time-frequency signal analysis approach heavily depends on the problem at hand, since different approaches may not yield the same estimate of the energy distribution on the time-frequency plane for the same signal (e.g. [38, 39]).

The CWT is a versatile joint time-frequency signal analysis tool which measures the similarity between a signal and a mother wavelet, providing a time-scale representation of the examined signal. Since there is a direct relationship between scales and frequencies, the CWT can also be expressed with a time-frequency representation. Moreover, the mother wavelet provides a flexible time-frequency window that is automatically narrowed for detecting the rapidly changing details of high-frequency phenomena and widened for capturing the slowly changing details of signals. This localization property makes the CWT a powerful tool for analyzing signals with transient features, like seismic ground motions. The CWT method is able to provide a robust representation of the energy evolution in time and with a high resolution in the time-frequency plane.

The paper presents a novel site and spectrum-based stochastic methodology for the generation of bidirectional horizontal fully nonstationary ground motion components using the CWT. Regarding the ground motion simulation procedure, the proposed approach combines well-established tools such as the SRM in conjunction with the CWT method, in order to extract and exploit temporal and frequency characteristics from seismic ground motions recorded at the site of interest. Specifically, the proposed methodology operates in the time-frequency domain in order

to produce fully nonstationary signals through a nonseparable process. Notably, the time-frequency analysis is applied for the whole accelerogram generation procedure rather than the PSD function modeling specifically as in [26].

The proposed methodology follows the rationale of evolutionary spectrum techniques that use an EPSD function where the amplitude and spectral nonstationarity is modeled by modifying a stationary signal with a time-frequency modulating function (e.g. [16, 18]). In the proposed approach, the time-frequency modulating function is extracted from a seed record using the time-frequency representation obtained with the aid of the CWT method. It is noted that the seed record is not added to the stationary component like in [14]; it is used only for modeling the time-frequency modulating function. Spectrum compatibility is ensured with the aid of the SRM when generating the stationary signal. Therefore, the proposed methodology can provide any number of required site and spectrum-compatible seismic fully nonstationary accelerograms. It is important to note that the proposed methodology is independent of the choice of the acceleration spectrum that is used as target. Various response spectra can be chosen, depending on the problem at hand, for example the conditional mean spectrum (CMS) [40], or scenario-specific spectra obtained from ground motion models (GMMs). Furthermore, a number of pertinent current stochastic dynamics studies are based on excitations characterized by evolutionary power spectra generated compatible with modern aseismic code provisions [3, 5, 6].

The proposed methodology can be seen as an alternative to record selection. The method is free of the record scaling practice, which is always a controversial issue, while it can be quite useful when there is a lack of recorded signals. This is almost always the case when (unscaled) ground motions with large intensity are sought. Furthermore, the proposed model can be applied with the same rationale as other, well-known, ground motion selection procedures that use target spectra, for example, the method proposed by Jayaram et al. [41], or the recently proposed approach by Yanni et al. [16]. THA requires suites of acceleration records that represent the seismic actions as input. When the selection of multiple seed records is desired, it is possible to choose a small number of recorded accelerograms obtained either from the same site, that is, the site of interest, but from different earthquake events, or from a site with similar characteristics such as fault type, soil type, M_w–R, and so forth. These records can be randomly selected, as discussed in the *site and spectrum-based variant* in [16]. In this approach, suites of fully nonstationary artificial accelerograms that are compatible with a target spectral mean and a target variability for the whole period range are generated following a probabilistic procedure. More specifically, multiple target response spectra are produced from a random vector that follows the normal distribution and is statistically defined by the target spectral mean and variability by also considering the spectral correlation at pairs of periods. For each of these spectra, a corresponding spectrum-compatible artificial accelerogram can be generated, following the proposed wavelet-based procedure and using randomly sampled appropriate seed records.

The model is also extended to generate pairs of bidirectional horizontal components. Since the methodology is spectrum-compatible, this is achieved by defining two appropriate orthogonal target spectra whose geometric mean matches a target median spectrum obtained from a GMM. These spectra are generated using a probabilistic procedure that takes into account the correlation structure of spectral acceleration pairs in orthogonal directions at different periods, based on empirical models of practice [42]. Thus, a single-component ground motion may be used as a seed record, as the spectral correlation between the two components is already included in the model. Alternatively, two-component seed records may also be used. Once the orthogonal target spectra are obtained, the two artificial ground motion components are generated independently following the proposed methodology. An online tool that implements the proposed methodology is also freely provided at [43].

The proposed model has several advantages. The application of the CWT offers the advantage of a fine time-frequency resolution; thus, the modulus of the estimated coefficients is a robust representation of the signal's energy evolution in time. As a result, the extracted time-frequency modulating function offers a detailed and realistic representation of the nonstationary characteristics of the seed records. Furthermore, the fully nonstationary signals are directly modeled in the time-frequency domain, rather than being treated separately for the amplitude and frequency modulation, as found in several relevant studies in the literature [13, 26]. Additionally, the generated signals are unique rather than modified versions of the seed record. Moreover, the proposed methodology is straightforward, requiring only one seed record and a target spectrum as inputs, thus making it applicable to the engineering practice.

The approach proposed for the generation of bidirectional horizontal components offers the advantage that it is based on the probabilistic generation of appropriate orthogonal spectra that are then used for the simulation of bidirectional ground motions by employing a spectrum-based methodology. Therefore, it is an efficient procedure that can be combined with any provided seismic hazard scenario that is represented by a target acceleration spectrum, for example, a CMS, a GMM, or a design code spectrum. Moreover, it is not limited to the proposed accelerogram generation methodology; any site and spectrum-based methodology can be used instead. As mentioned, relative works in the literature [29, 30] focus on the statistical parameterization of online databases, thus they could be more cumbersome and highly dependent on databases' content. The proposed procedure also offers the advantage that a single-component ground motion may be used as a seed record. Alternatively, based on the availability, two-component seed records may also be used. Finally, it is noted that the proposed methodology is computationally efficient, since the generation of either single or bidirectional components is a straightforward task that is performed within a few seconds.

2 | Spectral Representation Method for Stationary Seismic Signals

Stationary and spectrum-compatible accelerograms can be generated as stochastic processes using the SRM. Following Shinozuka and Deodatis [32], the ground motion signal due to a seismic event can be modeled as a zero-mean stationary Gaussian stochastic process $a_s(t)$ of finite duration T_s and it is produced as

the superposition of harmonic components with random phase angles

$$a_s(t) = \sum_{i=1}^{N} \sqrt{2 G_s(\omega_i) \Delta \omega} \cos(\omega_i t + \theta_i) \tag{1}$$

where N is the number of harmonics to be superimposed, ω_i is the angular frequency of the ith harmonic, $\Delta\omega$ is the constant integration step, and θ_i are the random phase angles, uniformly distributed in the interval $[0, 2\pi]$. Moreover, the amplitude of each component is related to the one-sided PSD function $G_s(\omega_i)$ of the stochastic seismic motion, thus providing the basis for generating target spectrum-compatible signals. This can be achieved by determining $G_s(\omega_i)$ based on the random vibration analysis approach proposed by Vanmarcke and Gasparini [17] and further developed by Cacciola et al. [44]. The methodology relies on the evaluation of a one-sided PSD function $G_s(\omega_i)$ which is consistent with a target pseudo-acceleration response spectrum $S_a^*(\omega_i, \zeta)$ of a quiescent elastic single-degree-of-freedom (SDOF) oscillator of undamped angular frequency ω_i and damping ratio ζ, that is subjected to the generated signal $a_s(t)$. If $X_i(t)$ is the obtained stochastic response process, the pseudo-acceleration response spectrum is

$$S_a^*(\omega_i, \zeta) = \eta_{X_i} \omega_i^2 \sqrt{\lambda_{0, X_i}} \tag{2}$$

where η_{X_i} is the peak factor and λ_{0, X_i} is the variance of the stochastic response process $X_i(t)$. The peak factor η_{X_i} is the critical factor by which the standard deviation $\sqrt{\lambda_{0, X_i}}$ of the considered elastic oscillator response is multiplied to predict a level of spectral acceleration $S_a^*(\omega_i, \zeta)$, below which the peak response will remain in the interval of T_s, with probability p. The estimation of η_{X_i} is related to the concept of the first-passage problem. According to the hypothesis of a barrier outcrossing in clumps [45], the peak factor is

$$\eta_{X_i}(T_s, p) = \sqrt{2 \ln\left\{ 2 N_{X_i} \left[1 - e^{\left(-\delta_{X_i}^{1.2} \sqrt{\pi \ln(2 N_{X_i})}\right)} \right] \right\}} \tag{3}$$

where N_{X_i} is the mean zero crossing rate and δ_{X_i} is the spread factor of the stochastic response process $X_i(t)$, defined as

$$N_{X_i} = \frac{T_s}{2\pi} \sqrt{\frac{\lambda_{2, X_i}}{\lambda_{0, X_i}}} (-\ln p)^{-1} \quad \text{and} \quad \delta_{X_i} = \sqrt{1 - \frac{\lambda_{1, X_i}^2}{\lambda_{0, X_i} \lambda_{2, X_i}}} \tag{4}$$

where λ_{n, X_i} is the nth order ($n = 0, 1, 2$) spectral moment of the stochastic response process $X_i(t)$, evaluated as

$$\lambda_{n, X_i} = \int_0^\infty \frac{\omega^n}{(\omega_i^2 - \omega^2)^2 + (2\zeta\omega_i\omega)^2} G_s(\omega) d\omega \tag{5}$$

The evaluation of the target spectrum-compatible PSD function $G_s(\omega_i)$, depends on the peak factor, as well as on the variance of the SDOF response. Nevertheless, as indicated by Equations (3)–(5), these two parameters depend on the input $G_s(\omega_i)$ itself, thus requiring a solution of the inverse stochastic dynamics problem. Within this context, the variance λ_{0, X_i} of the response process

can be approximated as [34]

$$\lambda_{0, X_i} = \frac{G_s(\omega_i)}{\omega_i^3} \left(\frac{\pi}{4\zeta} - 1 \right) + \frac{1}{\omega_i^4} \int_0^{\omega_i} G_s(\omega) d\omega \tag{6}$$

Furthermore, Cacciola et al. [44] proposed that the mean zero crossing rate and the spread factor can be approximated with reference to a white-noise input [46] as

$$N_{X_i} = \frac{T_s}{2\pi} \omega_i (-\ln p)^{-1} \quad \text{and}$$

$$\delta_{X_i} = \sqrt{1 - \frac{1}{1 - \zeta^2} \left(1 - \frac{2}{\pi} \arctan \frac{\zeta}{\sqrt{1 - \zeta^2}} \right)^2} \tag{7}$$

Approximating the target PSD function with a constant piecewise function, the integral of Equation (6) can be obtained as a discrete summation. Replacing the obtained λ_{0, X_i} in Equation (2) leads to the following expression for the spectral acceleration $S_a^*(\omega_i, \zeta)$:

$$S_a^{*2}(\omega_i, \zeta) = \eta_{X_i}^2 G_s(\omega_i) \omega_i \left(\frac{\pi - 4\zeta}{4\zeta} \right)$$

$$+ \eta_{X_i}^2 \Delta\omega \left(\sum_{k=1}^{i-1} G_s(\omega_k) + G_s(\omega_i) \right) \tag{8}$$

Finally, the target spectrum-compatible one-sided PSD function $G_s(\omega_i)$ of the stationary process can be obtained solving Equation (8) with respect to $G_s(\omega_i)$ as follows:

$$G_s(\omega_i) = \begin{cases} \dfrac{4\zeta}{\omega_i \pi - 4\zeta \omega_{i-1}} \left(\dfrac{S_a^{*2}(\omega_i, \zeta)}{\eta_{X_i}^2} - \Delta\omega \displaystyle\sum_{k=1}^{i-1} G_s(\omega_k) \right), & \omega_i > \omega_0 \\ 0, & \omega_i \le \omega_0 \end{cases} \tag{9}$$

The range of ω_i is defined within the interval $[\omega_0, \omega_u]$, where ω_0 is the lowest frequency bound of the existence domain of Equation (3), and ω_u is an upper cut-off frequency beyond which the PSD function $G_s(\omega_i)$ is assumed to be zero for either mathematical or physical reasons. In Equation (7), the value of ω_0 is 0.36 rad/s [44] and cannot be lesser since it would make the quantity inside the root in Equation (3) negative. Furthermore, for $i = 1$, $G_s(\omega_1) = 0$ [32]. The accelerograms generated with Equations (1)–(9) are stationary and all have the same duration T_s.

3 | Time-Frequency Representation of Signals

3.1 | Signal Time-Frequency Analysis

Signal time-frequency analysis is a powerful tool for analyzing and interpreting signals whose spectral content varies with time. Traditional Fourier analysis provides insight into the frequency components of a signal, however, it lacks the ability to represent how these components evolve over time since this transform provides only the average spectral decomposition of the signal. Time-frequency analysis addresses this limitation by providing a representation of a signal simultaneously in both the time and the frequency domains. Various methods for performing time-frequency analysis exist, like the Short-Time Fourier Transform (STFT), the Wigner–Ville distribution, the Chirplet Transform,

the Wavelet Transform, the Hilbert–Huang Transform, and the S-Transform among others. Time-frequency analysis is crucial in various fields, enabling a deeper understanding of signal dynamics and supporting advanced signal processing tasks, as discussed in the Introduction.

The WT provides a multi-resolution analysis by decomposing the signal into a set of basis functions called wavelets, which can be scaled and shifted. In the following section, we briefly discuss the CWT that is adopted for the purpose of this study. The choice of a time-frequency analysis method depends on the characteristics of the signal and the specific application. For instance, the STFT is suitable for signals with relatively stationary frequency content over short periods, while the CWT is more appropriate for signals with transient features, such as the case of seismic ground motions.

3.2 | The Continuous Wavelet Transform

The basic idea of the CWT is to use a set of basis functions known as wavelet family, formed by the dilation and translation of a prototype function known as mother wavelet $\psi(t)$. Although the CWT is available in various software, its results may vary considerably depending on various details that control the proper application of the method. Hence, a brief introduction to the method is provided, explaining also some of the assumptions that are made.

Let $\psi(t) \in L^1(\mathbb{R}) \cap L^2(\mathbb{R})$ be a window function of finite energy[1] that fulfills the admissibility conditions. This function is called the mother (or analyzing) wavelet, and the corresponding family of wavelets is the group $[\psi_{b,a}; b \in \mathbb{R}, a \in \mathbb{R}_+^*]$ of shifted and scaled copies of $\psi(t)$, defined as

$$\psi_{b,a}(t) = \frac{1}{\sqrt{a}} \psi\left(\frac{t-b}{a}\right) \qquad (10)$$

where $t \in \mathbb{R}$, a is a scaling parameter that defines the dilation of the mother wavelet $\psi(t)$, and b is the translation parameter related to time. The member of the family where $b = 0$ and $a = 1$ is the mother wavelet.

For a function $\psi(t)$ to be accepted as a mother wavelet, the admissibility condition must be fulfilled

$$C_\psi = \int_{-\infty}^{+\infty} \frac{\left|\widehat{\psi}(\omega)\right|^2}{\omega} d\omega < \infty \qquad (11)$$

where $\widehat{\psi}(\omega) = \int_{-\infty}^{+\infty} \psi(t)e^{-i\omega t} dt$ is the FT of $\psi(t)$, which implies that $\int_{-\infty}^{+\infty} \psi(t)dt = 0$ so that the graph in time is a small wave.

Let $u(t)$ be a signal that is of finite energy and a piece-wise continuous function of time. Using a mother wavelet $\psi(t)$, the CWT of the signal is given as

$$T_\psi[u](b,a) = \int_{-\infty}^{+\infty} u(t) \frac{1}{\sqrt{a}} \overline{\psi}\left(\frac{t-b}{a}\right) dt \qquad (12)$$

The symbol $\overline{\psi}$ denotes the complex conjugate of ψ. Equation (12) shows that CWT transforms a one-dimensional (time domain) signal $u(t)$ to a two-dimensional representation: the time-scale plane. The CWT, as defined by Equation (12), can be interpreted as the convolution of $u(t)$ with $\frac{1}{\sqrt{a}} \overline{\psi}\left(-\frac{b-t}{a}\right)$, or as the inner product of $u(t)$ with the shifted and scaled copies of the mother wavelet $\frac{1}{\sqrt{a}} \psi\left(\frac{t-b}{a}\right)$. Alternatively, using Parseval's identity, the CWT can be equivalently estimated through the Fast Fourier Transform algorithm by using the following equation:

$$T_\psi[u](b,a) = \frac{\sqrt{a}}{2\pi} \int_{-\infty}^{+\infty} \widehat{u}(\omega)\overline{\widehat{\psi}}(a\omega)e^{i\omega b} d\omega \qquad (13)$$

where $\widehat{u}(\omega) = \int_{-\infty}^{+\infty} u(t)e^{-i\omega t} dt$ is the FT of $u(t)$ and $\widehat{\psi}(\omega)$ is the mother wavelet defined in the frequency domain.

When the admissibility condition of Equation (11) is satisfied, the original signal $u(t)$ may be reconstructed using the finite constant C_ψ

$$u(t) = \frac{1}{C_\psi} \int_{-\infty}^{+\infty} \int_0^{+\infty} T_\psi[u](b,a) \frac{1}{\sqrt{a}} \psi\left(\frac{t-b}{a}\right) \frac{da}{a^2} db \qquad (14)$$

The term $1/\sqrt{a}$ in Equations (10), (12), (14) is a normalizing factor. The CWT definitions in the literature vary slightly depending on the chosen wavelet normalization. For the purposes of this study, the $L^2(\mathbb{R})$ normalization [47, 48] was employed, as will be explained in Section 5.1.

There is a direct relationship between the scales a and the angular frequencies ω. More specifically, values of $0 < a < 1$ result in a more compressed wavelet, allowing the detection of the high-frequency content of the signal. On the other hand, large values of $a > 1$ result in a more stretched wavelet, which detects the low-frequency content of the signal.

Therefore, the quantity $1/a$ can be assimilated to a frequency parameter ω by setting $\omega = \omega_\psi^*/a$. There are several representations of ω_ψ^* in the literature. One of the most common definitions is that ω_ψ^* is the center frequency and it is equal to the frequency that maximizes the FT of the wavelet modulus ω_ψ^0, that is $\omega_\psi^0 = \arg\max(|\widehat{\psi}(\omega)|)$. Two other definitions classically found in literature, are the energy frequency $\bar{\omega}_\psi$ and the time-varying instantaneous frequency of the wavelet at its time center $\ddot{\omega}_\psi(0)$. More details can be found in [49]. For this study, ω_ψ^* is defined as the wavelet center frequency.

4 | Generation of single-component ground motions

The proposed methodology employs the CWT to generate site- and spectrum-compatible fully nonstationary artificial accelerograms. The method relies on the generation of a stationary and spectrum-compatible ground motion using the SRM, which is then processed in the time-frequency domain using the CWT method in order to become fully nonstationary. The modulus of the CWT is a robust representation of the signal's energy
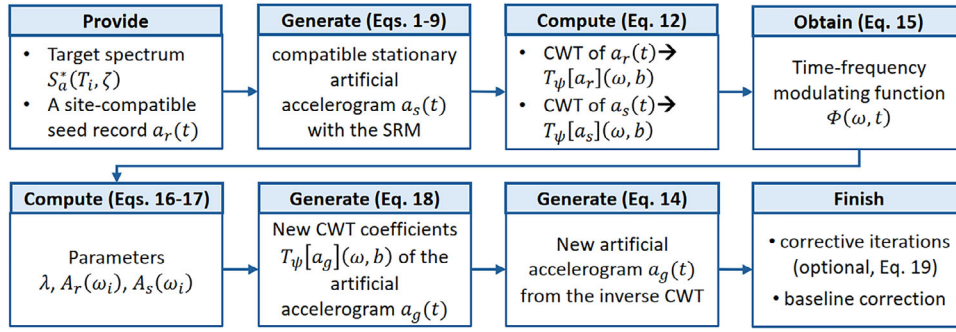
FIGURE 1 | Flowchart of the proposed wavelet-based procedure for generating single site and spectrum-compatible fully nonstationary artificial ground motions.

evolution in time. Consequently, the amplitude and frequency modulation is modeled using a time-frequency modulating function derived from the modulus of the CWT coefficients of a site-compatible recorded ground motion.

The proposed methodology consists of a few simple steps. First, the desired target spectrum and the peak ground acceleration (PGA) are determined. Next, a recorded accelerogram is selected from the site of interest and is analyzed in the time-frequency domain following the CWT method. The time-frequency modulating function is then obtained from the $L^2(\mathbb{R})$ normalized modulus of the obtained CWT coefficients (Equation 12), leading to a realistic representation of the time-varying spectral energy distribution. A zero mean and spectrum-compatible stationary Gaussian stochastic process is then generated using the SRM [32, 44]. This component is also the one that defines the phase distribution of the final accelerogram. Spectrum compatibility is ensured through the PSD function of the stationary process. The generated stationary signal is then converted to the time-frequency domain using the CWT.

Next, the obtained time-frequency modulating function modifies accordingly the stationary stochastic process in the time-frequency domain, and updated CWT coefficients are estimated. The produced signal is then transformed back into the time domain using the inverse CWT and the new artificial accelerogram is obtained. A few corrective iterations in the frequency domain may be required in order to achieve perfect spectrum matching, especially at the low-frequency range, depending on the shape of the target spectrum and the time-frequency modulation of the seed record. The above steps are discussed in detail in the sections that follow[2] and summarized in the flowchart of Figure 1. The online tool for the proposed methodology is freely available at [43].

4.1 | Time-Frequency Modulating Function

Initially, the target spectrum $S_a^*(\omega_i, \zeta)$, frequency range $[\omega_0, \omega_u]$, as well as the mother wavelet are defined/selected. A past-recorded ground motion $a_r(t)$ is selected, compatible with the site of interest. The total duration t_f and the PGA_r are also extracted from the seed record. The signal is then analyzed in the time-frequency domain using the CWT, with a fine frequency resolution, in order to obtain the CWT coefficients $T_\psi[a_r](\omega, b)$

according to Equation (12), and their modulus $\left|T_\psi[a_r](\omega, b)\right|$ is estimated. The time-frequency modulating function $\Phi(\omega, t)$ is defined as the normalized modulus of the CWT coefficients so that the peak of the function is equal to one

$$\Phi(\omega, t) = \frac{\left|T_\psi[a_r](\omega, b)\right|}{\max\left(\left|T_\psi[a_r](\omega, b)\right|\right)} \quad (15)$$

4.2 | Generation of Fully Nonstationary Ground Motions

A stationary, spectrum-compatible artificial accelerogram $a_s(t)$ is generated following Equations (1)–(9), based on the target spectrum $S_a^*(\omega_i, \zeta)$, the frequency range $[\omega_0, \omega_u]$, and a total duration in agreement with the corresponding duration of the seed record ($T_s = t_f$). The generated signal $a_s(t)$ is then analyzed in the time-frequency domain using the CWT (Equation 12), with the same filter bank as the seed record. Thus, the wavelet coefficients $T_\psi[a_s](\omega, b)$ are estimated. In order to ensure spectral energy distribution compatibility, the parameters λ, $A_s(\omega_i)$, and $A_r(\omega_i)$ are calculated. Specifically, λ is the ratio of the peak ground acceleration of the $a_s(t)$ signal (PGA_s) to the PGA_r

$$\lambda = \frac{PGA_s}{PGA_r} \quad (16)$$

and $A_s(\omega_i)$, and $A_r(\omega_i)$ is the area under the modulus of the CWT coefficients of the $a_s(t)$ and $a_r(t)$ signals, respectively, calculated along the time axis at every frequency ω_i:

$$A_s(\omega_i) = \int_0^{t_f} \left|T_\psi[a_s](\omega_i, b)\right| dt \quad \text{and}$$

$$A_r(\omega_i) = \int_0^{t_f} \left|T_\psi[a_r](\omega_i, b)\right| dt \quad (17)$$

The updated CWT coefficients that correspond to the artificially generated accelerogram are then computed at every frequency ω_i as

$$T_\psi[a_g](\omega_i, b) = T_\psi[a_s](\omega_i, b)\Phi(\omega_i, t)\frac{A_s(\omega_i)}{\lambda A_r(\omega_i)} \quad (18)$$
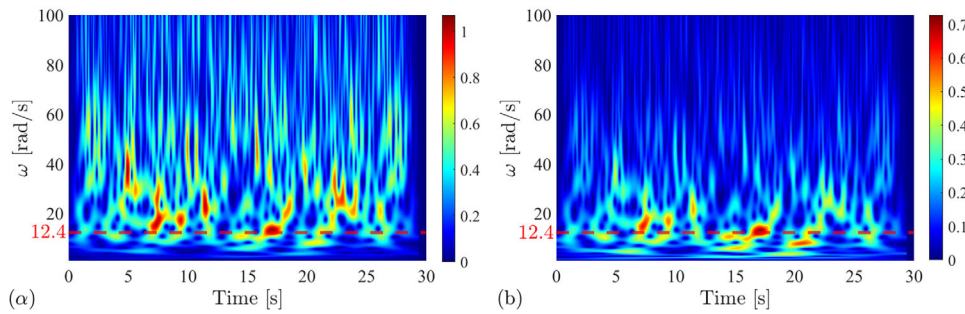
FIGURE 2 | Modulus plot of the CWT coefficients $\left|T_\psi[a_s](b,a)\right|$ of a stationary signal with one dominant frequency equal to 12.4 rad/s and noise: (a) using the $L^1(\mathbb{R})$ normalization, (b) using the $L^2(\mathbb{R})$ normalization.

Finally, the artificial site and spectrum-compatible accelerogram $a_g(t)$ is obtained by applying the inverse CWT on $T_\psi[a_g](\omega,b)$, using Equations (11) and (14).

4.3 | Post Processing

If fine spectrum compatibility is desired, corrective iterations can be carried out in the frequency domain. Thus, if $k = 1,\dots,N_{iter}$ where N_{iter} is the number of corrective iterations, the procedure is the following:

$$\left|F(\omega_i)^{(k+1)}\right| = \left|F(\omega_i)^{(k)}\right|\left[\frac{S_a^*(\omega_i,\zeta)}{S_a^{(k)}(\omega_i,\zeta)}\right] \text{ and}$$

$$\arg\left[F(\omega_i)^{(k+1)}\right] = \arg\left[F(\omega_i)^{(k)}\right] \tag{19}$$

where $F(\omega_i)^{(k)}$ is the FT of the generated accelerogram at the kth iteration, $S_a^*(\omega_i,\zeta)$ is the target spectrum, and $S_a^{(k)}(\omega_i,\zeta)$ is the response spectrum of the generated record at the kth iteration. Then, by applying the inverse FT, the signal is transformed back into the time domain, and a new time-history $a_g^{(k+1)}(t)$ is determined, along with its response spectrum $S_a^{(k+1)}(\omega_i,\zeta)$. Finally, baseline correction is applied in order to ensure realistic velocity and displacement time-histories. In this work, a simple quadratic curve is adopted.

5 | Further Discussion on the Application of the CWT Method

5.1 | Normalization

When applying the CWT, the wavelet $\psi_{b,a}(t)$ is normalized in order to ensure that the CWT coefficients at every scale a are directly comparable to each other and to the transforms of other time series. Different normalizations can be found in the literature. Normalizing by the term $1/\sqrt{a}$ in Equations (10), (12), and (14) ensures that all the scaled wavelets $\psi_{b,a}(t)$ will maintain the same energy. This is known as the $L^2(\mathbb{R})$ normalization of the CWT method and it is appropriate in cases where it is desired that the modulus-squared wavelet transform reflects the energy distribution of the analyzed signal. Due to this property, this definition of CWT has been used in various works that focus on estimating the evolutionary power spectrum using wavelets,

for example [50]. Alternatively, the normalizing factor can be defined as $1/a$, known as the $L^1(\mathbb{R})$ normalization. This term is appropriate when it is desired that the magnitude of the modulus of the wavelet transform reflects the amplitude of the analyzed signal. This definition is preferred in other civil engineering applications like structural damage detection [49].

The proposed methodology requires the use of the $L^2(\mathbb{R})$ normalization as it offers a robust presentation of the energy distribution of the signal, which is required for the time-frequency modulating function obtained with Equation (15). On the other hand, the modulus of the CWT coefficients obtained with the $L^1(\mathbb{R})$ normalization preserves the amplitude of the frequency values of the signal's components [49]. Consequently, since nonstationarity refers to the signal's energy evolution in time and since the proposed methodology is based on a nonseparable time-frequency analysis with a time-frequency modulating function, the $L^2(\mathbb{R})$ normalization is the appropriate one to use. This can be showcased with a pertinent example: a stationary signal is generated following Section 2, with one dominant frequency in time equal to 12.4 rad/s. Noise is also added to the signal. The signal is then analyzed in the time-frequency domain with the CWT using the $L^1(\mathbb{R})$ normalization and the $L^2(\mathbb{R})$ normalization. Figure 2 shows the modulus of the CWT coefficients $\left|T_\psi[a_s](b,a)\right|$ for each case. As observed in Figure 2b, the dominant frequency of 12.4 rad/s is clearly identified in the energy concentration region of $\left|T_\psi[a_s](b,a)\right|$ using the $L^2(\mathbb{R})$ normalization. In contrast, the $L^1(\mathbb{R})$ normalization in Figure 2a shows not only the dominant frequency but also a significant presence of noise.

5.2 | Choice of Mother Wavelet

The choice of the mother wavelet is essential for the CWT method. This choice is dictated by the characteristics of the signal under study and the application. The factors considered include the shape, the width, and so forth, of the mother wavelet, and more importantly, the definition of its function as real, analytic, or complex [51]. A complex mother wavelet will return information about both amplitude and phase and is better adapted for capturing oscillatory behavior. The analytic mother wavelets are complex functions whose frequency domain contains only positive frequencies, that is $\hat{\psi}(\omega) = 0 \,\forall\, \omega < 0$. Thus, analytic mother wavelets are more appropriate for the analysis of seismic signals.

Several functions have been proposed as mother wavelets in the literature such as the widely used Morlet wavelet, the Cauchy–Paul, the Shannon, and so forth. More recently, the generalized Morse wavelets [52] have been introduced as a "superfamily" defined in the frequency domain, from which all known analytic wavelets can be derived by appropriately adjusting two parameters β and γ that control the shape

$$\hat{\psi}_{\beta,\gamma}(\omega) = c_{\beta,\gamma}\omega^\beta e^{-\omega^\gamma}H(\omega) \tag{20}$$

where $c_{\beta,\gamma}$ is a normalization constant and $H(\omega)$ is the unit step function.

Since the signals that are analyzed in this study are seismic, analytic mother wavelets that have a wave-like shape and a relatively increased number of oscillation cycles are more appropriate in order to capture the signal's features. Two possible analytic mother wavelets are the Morlet wavelet and the Cauchy–Paul wavelet. The analytic Morlet wavelet is defined in the frequency domain as

$$\hat{\psi}(\omega) = \delta\sqrt{2\pi}e^{-(\omega-\omega_0)^2\delta^2/2} \tag{21}$$

where ω_0 is a frequency parameter controlling the number of oscillation cycles of the wavelet and δ is a parameter that controls the spread of the wavelet. The Morlet wavelet is only numerically admissible and analytic when the product of the two parameters, $\omega_0\delta$, is large enough ($\omega_0\delta \geq 5$ in practice). It is also noted that $\omega_0 = \omega_\psi^*$. The Cauchy wavelet of order ν is defined in the frequency domain as

$$\hat{\psi}(\omega) = 2\left(\frac{2\pi e}{\nu}\right)^\nu \omega^\nu e^{-\omega}H(\omega) \tag{22}$$

and $\nu = \omega_\psi^*$. With respect to Equation (20) the analytic Morlet wavelet can be derived for $\gamma = 3$ with an appropriate β value and the Cauchy–Paul wavelet for $\gamma = 1$ and $\beta = \nu$.

6 | Bidirectional Ground Motion Components

6.1 | Generation of Bidirectional Artificial Ground Motions

Seismic ground motions are often recorded by triaxial accelerographs; thus, in practice, every record contains two horizontal components and one vertical. The azimuths of the horizontal components are typically placed arbitrarily, often parallel to the north or to a known local fault. The methodology proposed in Section 4 is here extended in order to generate bidirectional horizontal components $a_x(t)$ and $a_y(t)$. Since the presented model is spectrum-compatible, this can be achieved by generating pairs of ground motions using two appropriate orthogonal response spectra whose geometric mean matches the target spectrum.

GMMs typically provide the geometric mean of the horizontal spectral accelerations rather than a particular component. If the two horizontal directions are set as x and y, then the geometric mean spectral accelerations $S_a^*(T_i, \zeta)$ at every period T_i are derived from the two horizontal components $S_{a,x}^*(T_i, \zeta)$ and

$S_{a,y}^*(T_i, \zeta)$ as

$$S_a^*(T_i, \zeta) = \sqrt{S_{a,x}^*(T_i,\zeta)S_{a,y}^*(T_i,\zeta)} \tag{23}$$

In ground motion selection techniques, Equation (23) is an adequate criterion for the selection of appropriate records. However, in a ground motion generation framework, the inverse problem has to be solved: the two components $S_{a,x}^*(T_i, \zeta)$ and $S_{a,y}^*(T_i, \zeta)$ are unknown, and they must be derived from a target $S_a^*(T_i, \zeta)$ spectrum obtained from a GMM. In order to achieve this, an appropriate probabilistic procedure is proposed, taking into account the correlation structure of spectral acceleration pairs in orthogonal directions at different periods following empirical models such as the one presented by Baker and Jayaram [42]. Specifically, pairs of $S_{a,x}^*(T_i, \zeta)$ and $S_{a,y}^*(T_i, \zeta)$ are generated for several trials and the best pair is selected based on three conditions/constraints that take into account the spectral acceleration values, as well as the spectral correlation coefficient $\rho_{S_{a,x}(T), S_{a,y}(T)}$.

Once the target spectra $S_{a,x}^*(T_i, \zeta)$ and $S_{a,y}^*(T_i, \zeta)$ are obtained, the bidirectional artificial acceleration time-histories $a_x(t)$ and $a_y(t)$ are generated, independently, following the content of Section 4. As the bidirectional characteristics are modeled by the target spectra, only one seed record may be used in order to generate the two-component horizontal ground motions; however, two horizontal components from the same record may also be selected as seeds instead. Concerning the temporal correlation $\rho_{a_x(t), a_y(t)}$ between the pair of generated ground motions $a_x(t)$ and $a_y(t)$, the only constraint is that it should be less than 0.30, according to the NIST GCR 11-917-15 [53], which is based on the results observed in several studies. Thus, a final check is performed that $\rho_{a_x(t), a_y(t)} < 0.30$, where $\rho_{a_x(t), a_y(t)}$ is the Pearson's correlation coefficient (PCC) of $a_x(t)$ and $a_y(t)$:

$$\rho_{a_x(t), a_y(t)} = \frac{\mathbb{E}\left[(a_x(t) - \mu_{a_x(t)})(a_y(t) - \mu_{a_y(t)})\right]}{\sigma_{a_x(t)}\sigma_{a_y(t)}} \tag{24}$$

where $\mu_{a_x(t)}$, $\mu_{a_y(t)}$ and $\sigma_{a_x(t)}$, $\sigma_{a_y(t)}$ are the mean and the standard deviation of $a_x(t)$ and $a_y(t)$, respectively, and $\mathbb{E}[\cdot]$ is the expectation operator. The above steps are summarized in the flowchart of Figure 3. The online tool for the proposed methodology is freely available at [43].

6.2 | Generation of Bidirectional Target Spectra

The proposed derivation is based on the empirically verified assumption that the geometric mean spectral accelerations at every period provided by the GMMs follow the log-normal distribution [54]. Consequently, the spectral accelerations at every period of a component with an arbitrary orientation will also follow the log-normal distribution. GMMs provide the logarithmic means $\ln[S_a^*(T_i, \zeta)]$ and standard deviations $\sigma_{\ln(S_a)}^*(T_i, \zeta)$ for the whole period range of interest, enabling the probabilistic modeling of $S_{a,x}^*(T_i, \zeta)$ and $S_{a,y}^*(T_i, \zeta)$. Furthermore, a correlation structure must be implemented for the spectral acceleration values of the two orthogonal directions at different periods. These assumptions allow for the estimation of $S_{a,x}^*(T_i, \zeta)$ and $S_{a,y}^*(T_i, \zeta)$ as

$$\ln\left[S_{a,x}^*(T_i, \zeta)\right] = \ln\left[S_a^*(T_i, \zeta)\right] + a_{i,x}\sigma_{\ln(S_a)}^*(T_i, \zeta) \quad \text{and}$$

$$\ln\left[S_{a,y}^*(T_i, \zeta)\right] = \ln\left[S_a^*(T_i, \zeta)\right] + a_{i,y}\sigma_{\ln(S_a)}^*(T_i, \zeta) \tag{25}$$
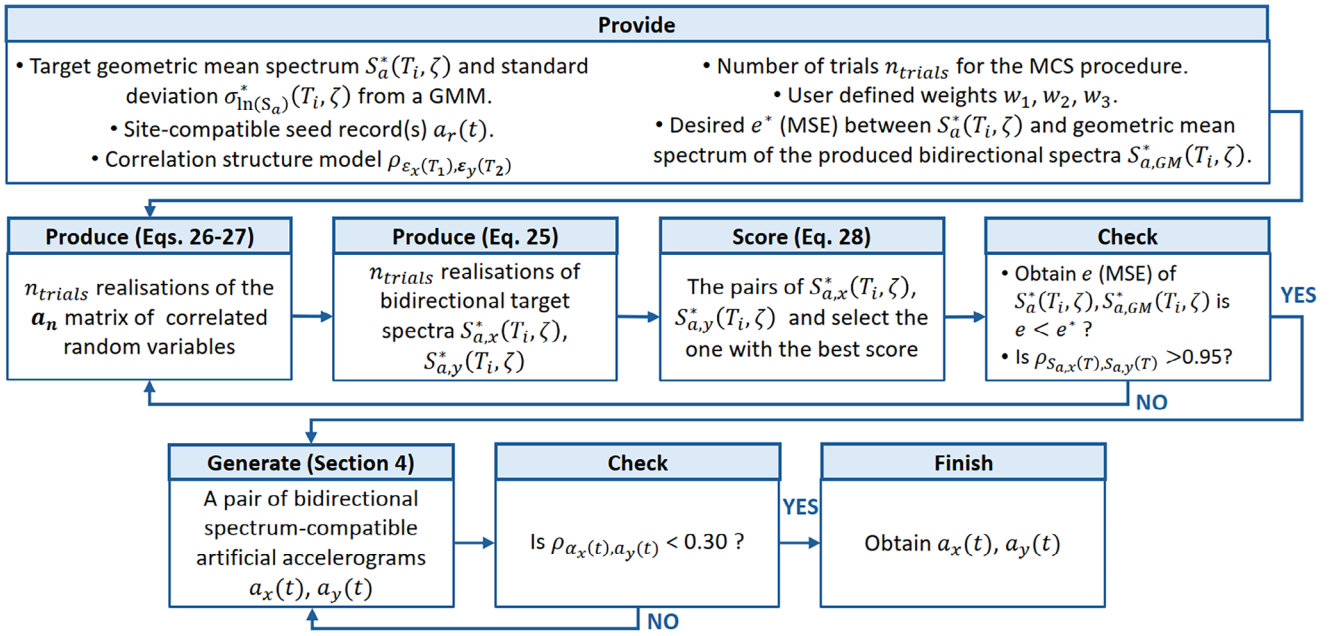
FIGURE 3 | Flowchart of the proposed wavelet-based procedure for generating bidirectional artificial acceleration time-histories.

where $a_{i,j}$ is a standard Gaussian random variable that integrates the correlations for spectral acceleration values at different periods in the x and y direction, $1 \leq i \leq N$, N is the number of period values considered, and j denotes the direction of the component, that is $j = x, y$. If $a_{i,x}, a_{i,y}$ are set as $\boldsymbol{a_n} = [a_{i,x}, a_{i,y}]$, then $\boldsymbol{a_n}$ is generated as a $N \times 2$ matrix that follows a standard multivariate normal distribution and each element $a_{i,j}$ refers to the ith period of the jth direction. The correlation between spectral acceleration values in orthogonal directions at different pairs of periods (T_1, T_2) is expressed through the $N \times N$ correlation matrix $\boldsymbol{\rho_{ln}}$. This matrix can be obtained from available empirical correlation models, like the model of Baker and Jayaram [42], where

$$\rho_{\varepsilon_x(T_1), \varepsilon_y(T_2)} = \rho_{\varepsilon(T_1), \varepsilon(T_2)}(0.79 - 0.023 \ln \sqrt{T_1 T_2}) \quad (26)$$

where $\rho_{\varepsilon(T_1), \varepsilon(T_2)}$ are the correlations between spectral accelerations at pairs of periods $S_{a,j}^*(T_1, \zeta), S_{a,j}^*(T_2, \zeta)$ for the same direction j, here obtained by [42]. Thus, if $T_{max} < 0.109$, $\rho_{\varepsilon(T_1), \varepsilon(T_2)} = C_2$, else if $T_{min} > 0.109$, $\rho_{\varepsilon(T_1), \varepsilon(T_2)} = C_1$, else if $T_{max} < 0.2$, $\rho_{\varepsilon(T_1), \varepsilon(T_2)} = \min(C_2, C_4)$, else $\rho_{\varepsilon(T_1), \varepsilon(T_2)} = C_4$, where $T_{min} = \min(T_1, T_2)$ and $T_{max} = \max(T_1, T_2)$. The correlated random realizations of $a_{i,j}$ that follow the standard normal distribution for the jth direction are generated as

$$\boldsymbol{a_j} = 0 + \boldsymbol{Lz} \quad (27)$$

where the vector $\boldsymbol{a_j}$ corresponds to the jth column of the $\boldsymbol{a_n}$ matrix, and $\boldsymbol{z}$ is a vector of uncorrelated random variables that follow the standard normal distribution. The matrix $\boldsymbol{L}$ is obtained from the Cholesky decomposition of the correlation matrix as $\boldsymbol{\rho_{ln}} = \boldsymbol{LL}^T$.

In order to select a pair of spectral components $S_{a,x}^*(T_i, \zeta)$ and $S_{a,y}^*(T_i, \zeta)$ whose geometric mean $S_{a,GM}^*(T_i, \zeta)$ matches the target $S_a^*(T_i, \zeta)$ best, an MCS procedure is adopted. Specifically, pairs of $S_{a,x}^*(T_i, \zeta)$ and $S_{a,y}^*(T_i, \zeta)$ are generated for a number of trials n_{trials} following Equations (25)–(27). For each trial, the geometric

spectral mean $S_{a,GM}^*(T_i, \zeta)$ is estimated and the best pair is selected using a scoring procedure based on the following three conditions

i. The mean squared error (MSE)[3] between the $S_{a,GM}^*(T_i, \zeta)$ and $S_a^*(T_i, \zeta)$ pairs is the smallest of n_{trials}. Additionally, a threshold can be also applied for the accepted MSE of the pairs.

ii. The spectral values of a component cannot significantly deviate from $S_a^*(T_i, \zeta)$.

iii. Since the two components correspond to the same event, a strong positive correlation is expected between the values of $S_{a,x}^*(T_i, \zeta)$ and $S_{a,y}^*(T_i, \zeta)$. Thus a condition of the spectral correlation coefficient $\rho_{S_{a,x}(T), S_{a,y}(T)} > 0.95$ is set, where $\rho_{S_{a,x}(T), S_{a,y}(T)}$ is the PCC of $S_{a,x}(T)$ and $S_{a,y}(T)$.

The first two conditions are reflected in the score estimation as

$$score = w_1 \frac{\sum_{i=1}^{N} \left| S_{a,GM}^*(T_i, \zeta) - S_a^*(T_i, \zeta) \right|^2}{N}$$
$$+ w_2 \frac{\max \left| S_{a,x}^*(T_i, \zeta) - S_a^*(T_i, \zeta) \right|}{S_a^*(T_i, \zeta)}$$
$$+ w_3 \frac{\max \left| S_{a,y}^*(T_i, \zeta) - S_a^*(T_i, \zeta) \right|}{S_a^*(T_i, \zeta)} \quad (28)$$

where w_1, w_2, w_3 are user-defined weights. It is recommended that the w_2, w_3 should be small compared to w_1.

7 | Numerical Applications

The efficiency of the proposed methodology is demonstrated with the help of two numerical applications. The first example focuses on the procedure of the generation of single-component fully
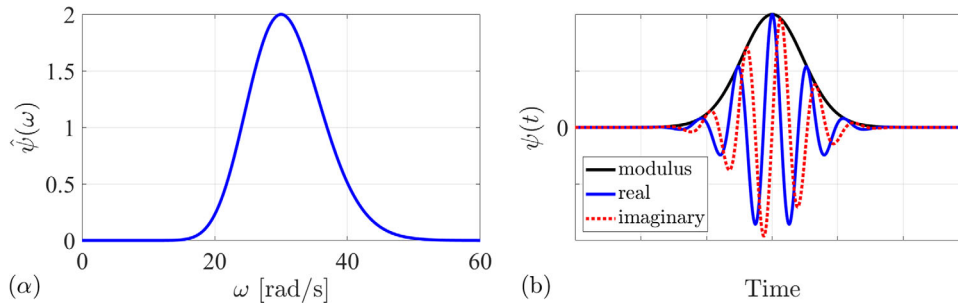
FIGURE 4 | The analytic Morlet wavelet of Equation (29) in (a) frequency domain representation, (b) time domain representation.

nonstationary artificial ground motions where the EC8 [55] spectrum is set as the target. The second example demonstrates the procedure for the generation of bidirectional fully nonstationary artificial accelerograms, where the median spectrum is obtained from a GMM. The error metric of spectrum matching is the MSE in both cases.

For the implementation of the CWT, the MATLAB Wavelet Toolbox [56] is used. For this work, the "cwt" command is used, with several modifications in order to achieve the $L^2(\mathbb{R})$ normalization. The analytic Morlet wavelet is selected as the mother wavelet for the CWT analysis. In the MATLAB Wavelet Toolbox, this wavelet is called through the "amor" command, which is a modified version of Equation (21) where all wavelets are also normalized to have maximum value $\hat{\psi}(\omega_\psi^*) = 2$. The wavelet parameters are fixed for $\omega_0 = 6$ and $\delta = \sqrt{2}$. The wavelet is defined in the frequency domain as

$$\hat{\psi}(\omega) = 2e^{-(\omega-6)^2/2}H(\omega) \tag{29}$$

The analytic Morlet wavelet of Equation (29) is shown in Figure 4.

7.1 | First Example: Generation of Single-Component Ground Motions

7.1.1 | Generation of Site-Compatible Artificial Accelerograms Matching a Design Code Spectrum

The site of interest is a region in central Greece, with soil conditions that correspond to type B soil according to EC8 [55] ($V_{S30} \approx 600$ m/s). Moreover, the target spectrum is the elastic EC8 spectrum, for damping ratio $\zeta = 5\%$, and $a_{gR} = 0.24$ g, thus the target PGA is equal to 0.288 g. The frequency range is chosen $[\omega_0, \omega_u] = [1, 125]$ rad/s, with frequency step $\Delta\omega = 0.12$.

The first step is to select a recorded accelerogram $a_r(t)$ from the site of interest that will be the seed record. The Kozani–Grevena 1995 time-history (Kozani station, Greece, 1995, L-component) is chosen from the PEER NGA-West 2 database [28]. The total duration of the accelerogram is $t_f = 29.39$ s, the PGA_r is 0.20 g, and the V_{S30} is 670 m/s. The seed record $a_r(t)$ is analyzed in the time-frequency domain, and the modulus of the CWT coefficients $\left|T_\psi[a_r](\omega, b)\right|$ is obtained and shown in Figure 5b,c. Following Equation (15), the time-frequency modulating function is determined from $\left|T_\psi[a_r](\omega, b)\right|$ and it is shown in Figure 6.

As observed, the time and frequency locations of the dominant features of the recorded accelerogram are preserved within the time-frequency modulating function.

For the next step, a stationary and spectrum-compatible accelerogram $a_s(t)$ is generated following the procedure presented in Section 2, for the target frequency range and total duration $T_s = t_f = 29.39$ s. The simulated signal is then analyzed in the time-frequency domain, with the same filter bank used for the CWT analysis of the recorded accelerogram. An example of a generated stationary accelerogram with its FT amplitude plot $|F(\omega)|$ and the modulus of the CWT coefficients $\left|T_\psi[a_s](\omega, b)\right|$ is shown in Figure 7. This component ensures the compatibility of the final accelerogram with the target spectrum. As observed, the dominant frequency is evident throughout the energy concentration region of the modulus plot. This is a direct result of the $L^2(\mathbb{R})$ normalization applied.

The parameters that ensure spectrum compatibility are subsequently estimated. Specifically, the coefficient λ is calculated, according to Equation (16). Moreover, the areas $A_s(\omega_i)$ and $A_r(\omega_i)$ are computed at every frequency ω_i, following Equation (17). Finally, Equation (18) is applied and the updated CWT coefficients $T_\psi[a_g](\omega, b)$ for the generated ground motion are obtained. The newly generated accelerogram $a_g(t)$ is produced by applying the inverse CWT on $T_\psi[a_g](\omega, b)$, following Equation (14). Due to the shape of the EC8 target spectrum and the frequency modulation of the seed record, one corrective iteration is needed for enhanced spectrum matching (Equation 19).

An example of a generated accelerogram is shown in Figure 8, along with its FT amplitude plot $|F(\omega)|$ and the modulus of the CWT coefficients $\left|T_\psi[a_g](\omega, b)\right|$. As observed in Figure 8, the produced accelerogram is fully nonstationary, as both temporal and frequency modulation is evident. Also, in comparison with Figure 5, it is observed that the energy distribution of the generated ground motions resembles that of the seed record. Specifically, the high-frequency components have a significant influence at the initial stages of the acceleration time-history, and they gradually diminish as time progresses, leading to a motion that is dominated by low-frequency components as it decays. This is in accordance with real seismic records, where typically the initial seconds of the motion are dominated by high-frequency P-waves, succeeded by moderate-frequency S-waves that dominate the strong-motion phase, and as the shaking progresses, low-frequency surface waves tend to dominate the
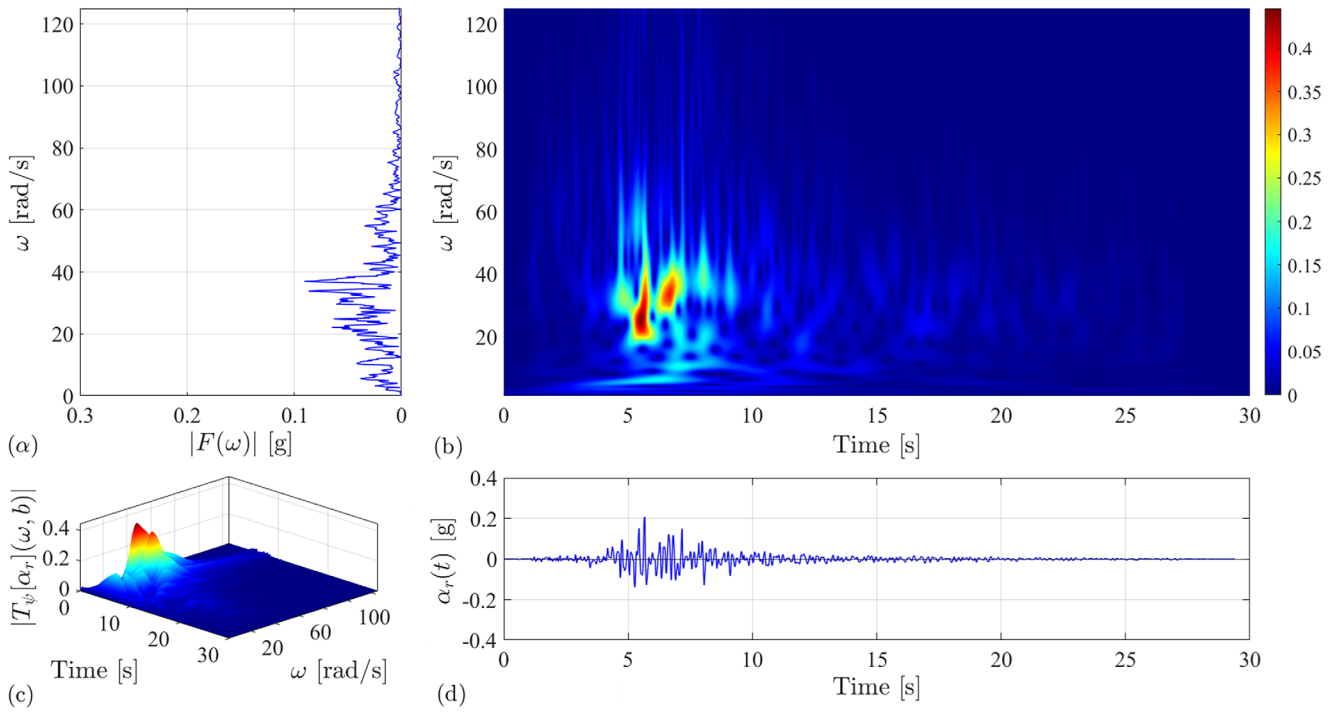
FIGURE 5 | The selected seed record: Kozani–Grevena 1995 earthquake, Greece, Kozani station, L-component: (a) $|F(\omega)|$ plot, (b) $\left|T_\psi[a_r](\omega, b)\right|$ two-dimensional plot, (c) $\left|T_\psi[a_r](\omega, b)\right|$ three-dimensional plot, (d) seed acceleration time-history.
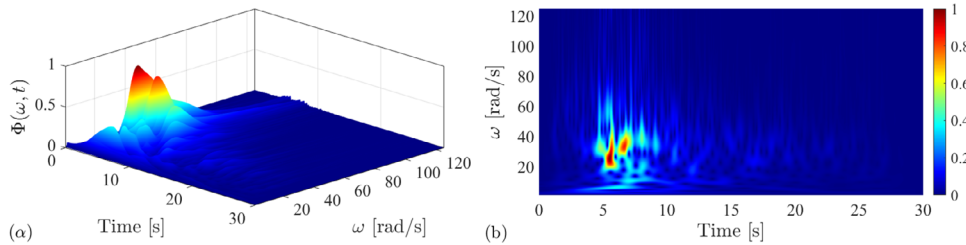

FIGURE 6 | The time-frequency modulating function, as extracted from the seed record of Figure 5: (a) three-dimensional plot, (b) two-dimensional plot in the time-frequency domain.

motion. A careful choice of the seed record is advisable. The seed record chosen should be representative of the site's seismicity and thus the use of "outliers" should be avoided. Furthermore, by comparing the FT amplitude plots in Figures 5, 7, and 8 it is observed that the frequency content of the records and the dominant frequency is modeled by the stationary signal. This characteristic is expected, as the stationary signal is the one that models the spectrum compatibility. Moreover, it is noted that the PGA of the generated ground motion is equal to 0.287 g which is very close to the target 0.288 g.

The comparison of the target EC8 elastic response spectrum $S_a^*(T_i, \zeta)$, with the seed record's response spectrum $S_a^r(T_i, \zeta)$, and the response spectrum $S_a(T_i, \zeta)$ of the generated accelerogram is shown in Figure 9a. Furthermore, Figure 9b shows the response spectrum of the produced accelerogram after one corrective iteration in comparison to the target EC8 elastic spectrum. As it is observed, there is a good matching of the $S_a(T_i, \zeta)$ of the original accelerogram to the target $S_a^*(T_i, \zeta)$, however not exact, due to the shape of the EC8 target spectrum and the frequency modulation

of the seed record. Therefore, a few corrective iterations can be applied for enhanced matching purposes. Finally, the consistency of the results is shown in Figure 10 where the Husid plots of 20 ground motions generated using the same procedure with the same inputs are shown, along with the respective mean m_{hp} and $\pm$ one standard deviation σ_{hp}. It is observed that there are no significant outliers in the sample[4].

7.1.2 | Influence of the Choice of Mother Wavelet

The efficiency of the proposed methodology has been examined considering other choices for the mother wavelet. For example, the Cauchy–Paul wavelet is employed. In the MATLAB Wavelet Toolbox, the particular wavelet is called through appropriate tuning of the "morse" command, which defines the Morse wavelet family of Equation (20). Thus, the Cauchy-Paul wavelet is called by setting $\gamma = 1$ and $\beta = \nu = \omega_\psi^*$, resulting in a modified version of Equation (22), where all wavelets are normalized to have maximum value $\widehat{\psi}(\omega_\psi^*) = 2$. For $\gamma = 1$ and $\beta = 12$, the
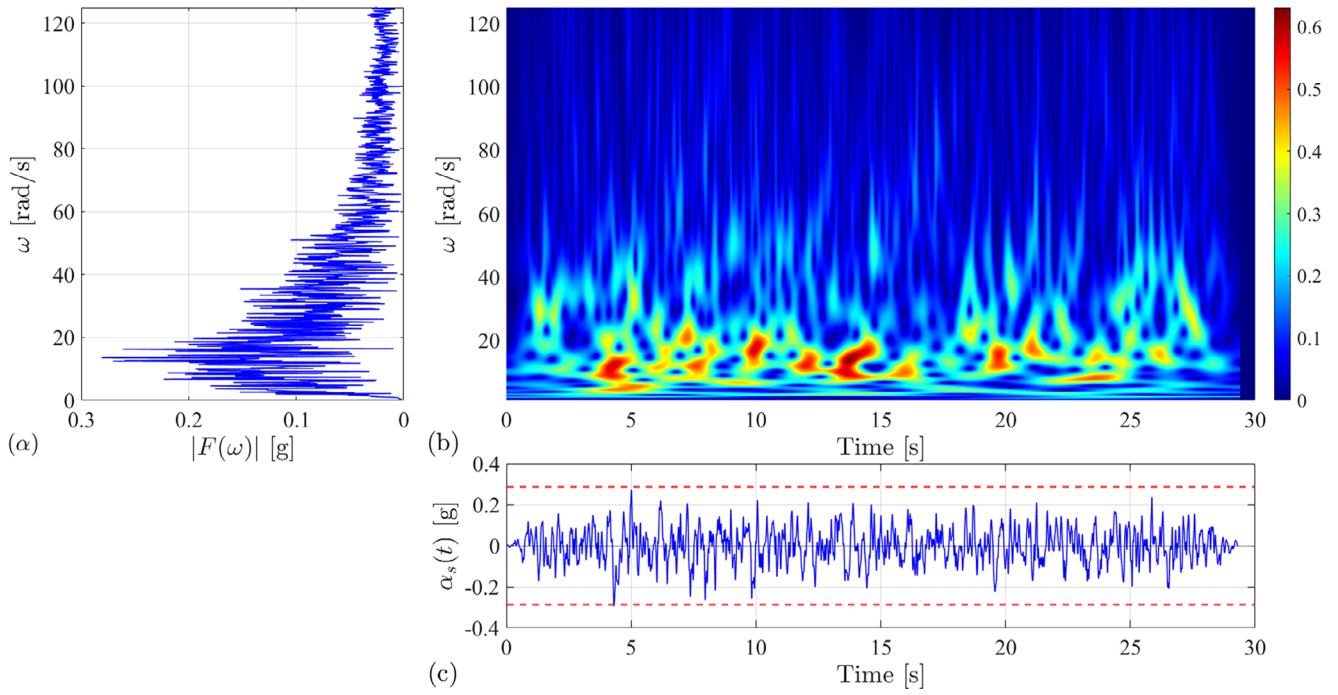
FIGURE 7 | A generated $a_s(t)$ stationary accelerogram with the SRM. (a) $|F(\omega)|$ plot, (b) $\left|T_\psi[a_s](\omega, b)\right|$ plot, (c) acceleration time-history. The target PGA is denoted with the red dashed line.
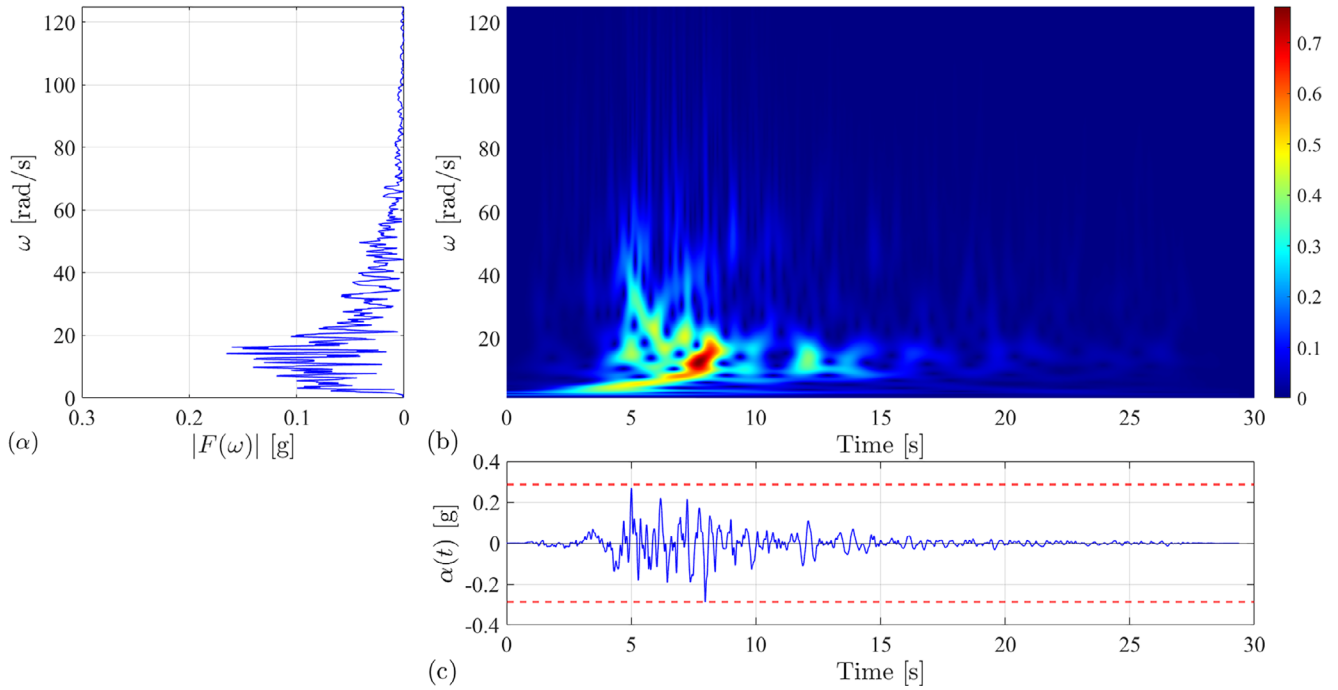

FIGURE 8 | An example of a generated single component fully nonstationary ground motion $a_g(t)$ with the proposed methodology. (a) $|F(\omega)|$ plot, (b) $\left|T_\psi[a_g](\omega, b)\right|$ plot, (c) acceleration time-history. The target PGA is denoted with the red dashed line.

wavelet is shown in Figure 11. Using this mother wavelet, the accelerogram generation procedure is repeated.

The generated ground motion is shown in Figure 12. It is observed that, compared to Figure 8, the number of cycles in the time domain is lesser, with a smaller number of peaks as well, resulting in a smaller strong motion duration. Moreover, one dominant

frequency is present within the signal, resulting in stationarity in the frequency domain. Furthermore, there is a lack of low frequencies dominating the latter part of the ground motion, thus the produced ground motion is not representative of real ground motions. These problems are attributed to the small number of oscillation cycles of the mother wavelet in the time domain, as seen Figure 11a. On the other hand, the spectrum matching is
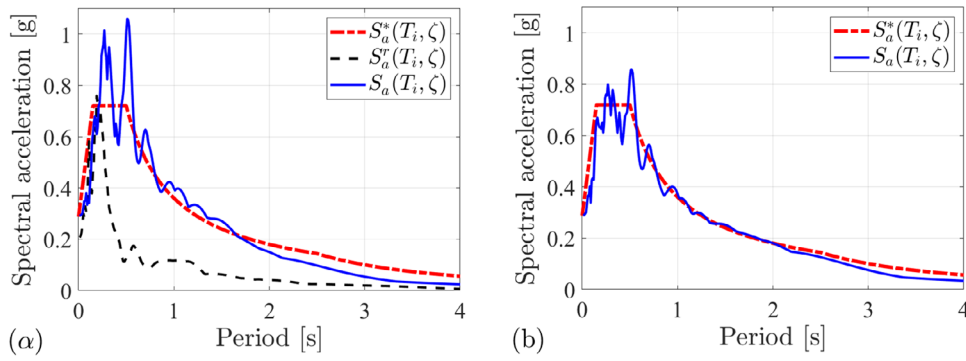
FIGURE 9 | (a) Comparison of the matching between the target EC8 elastic response spectrum $S_a^*(T_i,\zeta)$ with the seed record's response spectrum $S_a^r(T_i,\zeta)$ and the original generated accelerogram's response spectrum $S_a(T_i,\zeta)$, (b) Comparison of the matching between the target EC8 elastic response spectrum $S_a^*(T_i,\zeta)$ with the final accelerogram's response spectrum $S_a(T_i,\zeta)$ after one corrective iteration.
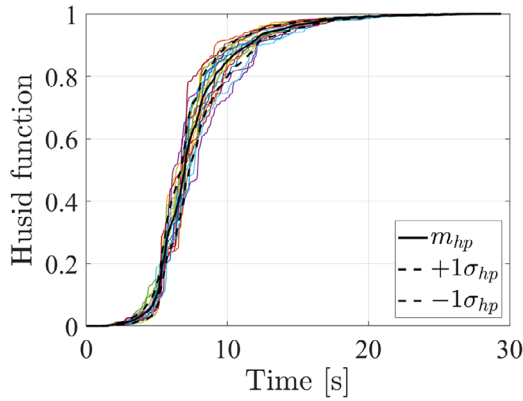

FIGURE 10 | Husid plot of 20 ground motions generated following the proposed methodology, with the same inputs, along with the respective mean m_{hp} and $\pm$ one standard deviation σ_{hp}.

very good, as seen in Figure 12c, where the target EC8 spectrum is compared to the generated ground motion response spectrum, without any corrective iterations. This is attributed to the fact that the center frequency of the selected mother wavelet $\omega_\psi^* = \nu = 12$ rad/s is very close to the dominant frequency of the stationary signal, equal to 12.54 rad/s, which is the counterpart responsible for the spectrum compatibility.

If the center frequency of the mother wavelet is increased, for example by setting $\nu = 30$ rad/s, the resulting mother wavelet has relatively a larger number of oscillation cycles, as shown in Figure 13. Using this mother wavelet, the accelerogram

generation procedure is repeated. The generated ground motion is shown in Figure 14. It is observed that the signal is fully nonstationary and the amplitude and frequency modulation is representative of real ground motions. Thus, a mother wavelet with an increased number of oscillation cycles models more effectively the nonstationarity of the generated signals. On the other hand, the spectrum matching is not that good as seen in Figure 14c, where the target EC8 spectrum is compared to the generated ground motion response spectrum, without any corrective iterations. This is attributed to the fact that the center frequency of the selected mother wavelet $\omega_\psi^* = \nu = 30$ rad/s is not close to the dominant frequency of the stationary signal, equal to 12.54 rad/s, which is the counterpart responsible for the spectrum compatibility. However, this issue can be easily corrected by applying one corrective iteration following Equation (19).

7.1.3 | Comparison With Other Spectrum-Compatible Methodologies

The proposed methodology is compared with another seed record based and spectrum-compatible model. Artificial accelerograms can be generated using a past-recorded accelerogram as a seed record by following the method proposed by Cacciola [14], where the fully nonstationary and spectrum-compatible accelerograms are generated by superimposing the natural record with a corrective term which is a stationary zero-mean Gaussian stochastic process, multiplied with a time-modulating function $\varphi(t)$. Thus, this model is comparable with the proposed methodology and they can have the same parameters set as target values and inputs.
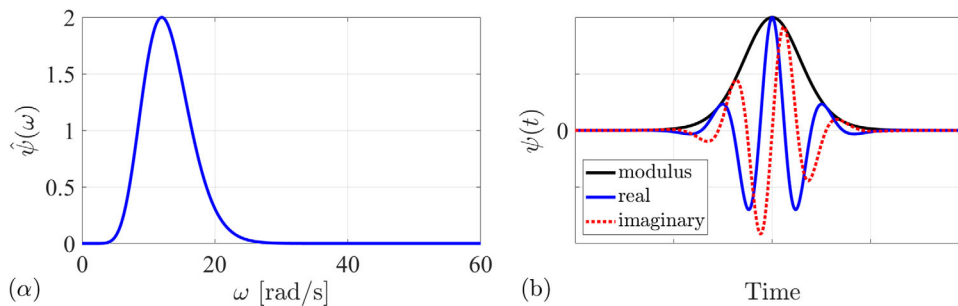

FIGURE 11 | The Cauchy–Paul wavelet defined from Equation (20) for $\gamma = 1$ and $\beta = 12$ in: (a) frequency domain representation, (b) time domain representation.
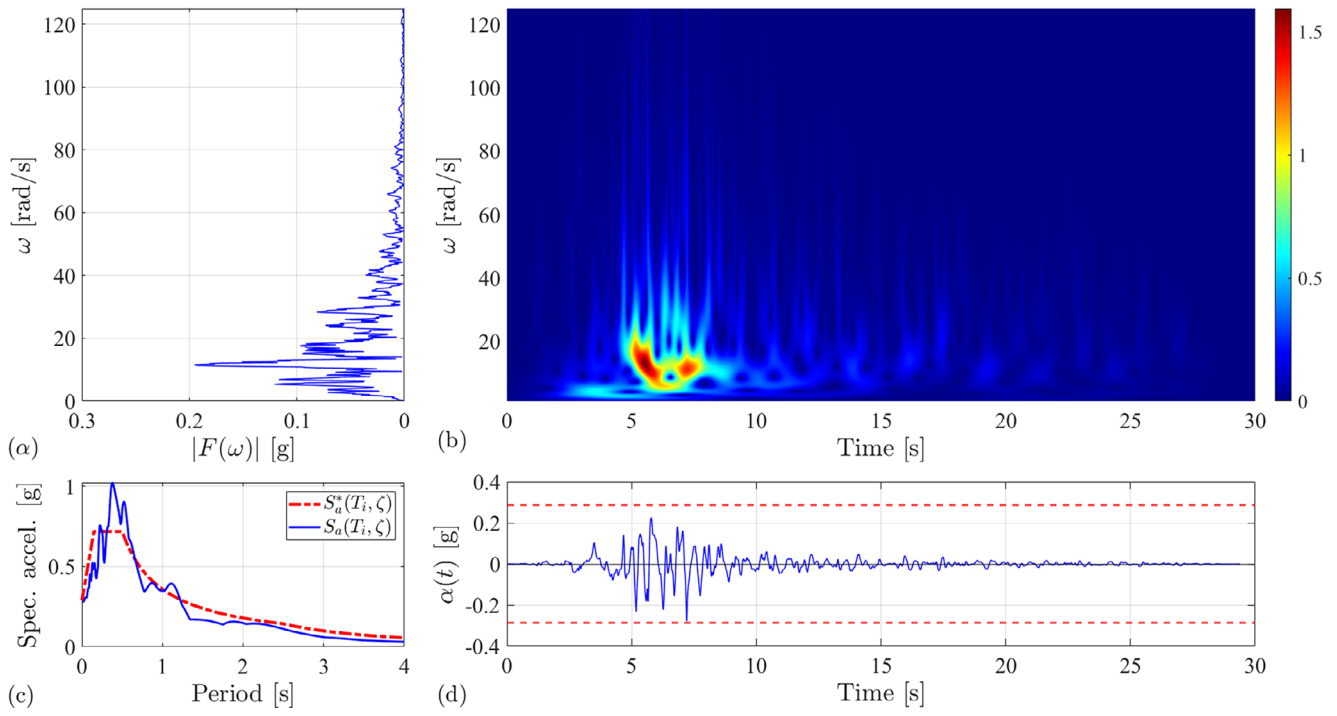
FIGURE 12 | A generated ground motion using the Cauchy-Paul wavelet of order $\nu = 12$: (a) $|F(\omega)|$ plot, (b) $\left|T_\psi[a](\omega, b)\right|$ plot, (c) matching comparison between the target EC8 elastic response spectrum $S_a^*(T_i, \zeta)$ and the generated accelerogram's response spectrum $S_a(T_i, \zeta)$, (d) acceleration time-history. The target PGA is denoted with the red dashed line.
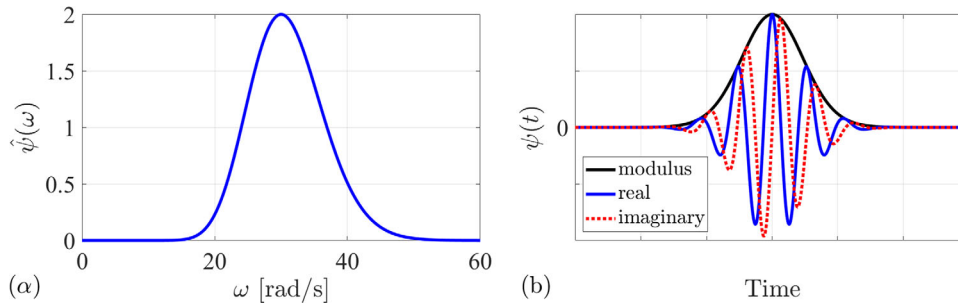

FIGURE 13 | The Cauchy–Paul wavelet defined from Equation (20) for $\gamma = 1$ and $\beta = 30$ in: (a) frequency domain representation, (b) time domain representation.

It is noted that in the proposed approach, the time-frequency modulating function is introduced based on the time-frequency representation of a seed record using the CWT. The seed record is not added to the stationary component like in [14], but it is used only for the modeling of the time-frequency nonstationarity. However, in both methodologies, the stationary part ensures compatibility with the target spectrum.

The Cacciola [14] methodology is applied for the same parameters and two corrective iterations following Equation (19), since they are needed for enhanced spectrum matching. The results are shown in Figure 15. For comparison purposes, the CWT of the generated ground motion is also plotted.

In comparison with Figures 8 and 14 it is observed that, for both models, the prominent energy concentration regions are within a similar time-frequency window. Furthermore, it is

observed that the FT amplitudes for both methodologies are mainly influenced by the stationary part, which is expected since it models the spectrum compatibility for both models. However, it is observed that there is a significant difference between the strong motion durations of the two models, as the Cacciola [14] model results in relatively larger values. This remark is essential since the strong motion duration is a very important characteristic of ground motions when non-linear response is expected and accumulation of damage is observed. Moreover, it is observed that the stationary component has the most influence on the generated record's time-frequency modulation, resulting in prominent high frequencies through almost all the signal's total duration. On the other hand, in the proposed model, the nonstationarity is mainly influenced by the seed record, resulting in prominent high-frequency components only at the initial stages of the acceleration time-history, which is in agreement with the nature of real ground motions.
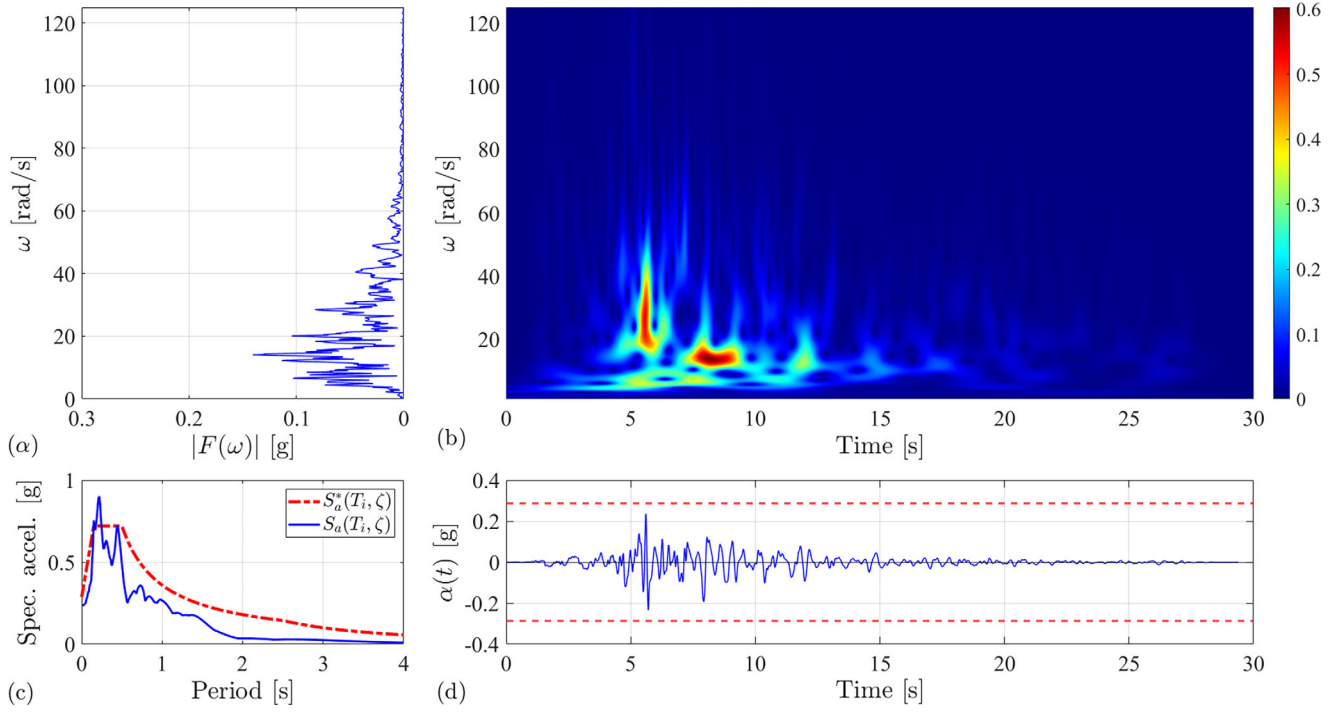
FIGURE 14 │ A generated ground motion using the Cauchy–Paul wavelet of order $\nu = 30$: (a) $|F(\omega)|$ plot, (b) $\left|T_{\psi}[a](\omega, b)\right|$ plot, (c) matching comparison between the target EC8 elastic response spectrum $S_a^*(T_i, \zeta)$ and the generated accelerogram's response spectrum $S_a(T_i, \zeta)$, (d) acceleration time-history. The target PGA is denoted with the red dashed line.
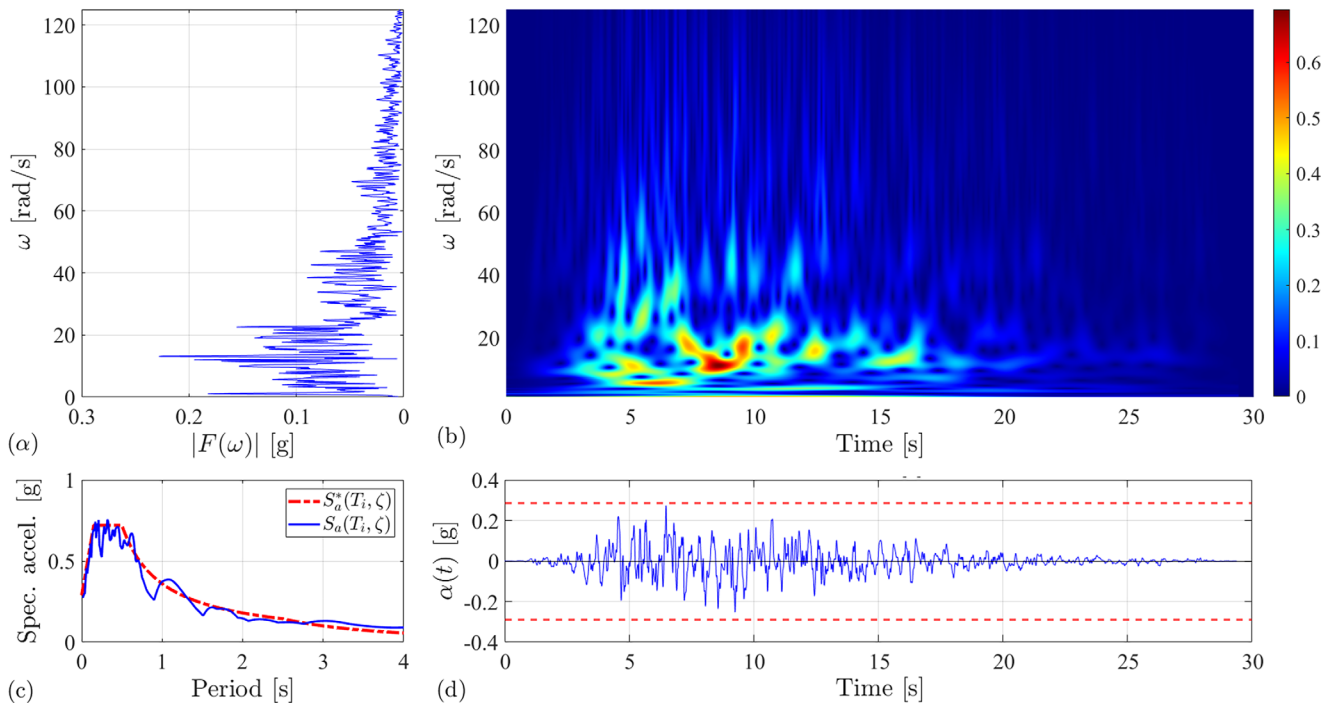

FIGURE 15 │ A generated ground motion using the Cacciola [14] methodology: (a) $|F(\omega)|$ plot, (b) $\left|T_{\psi}[a](\omega, b)\right|$ two-dimensional plot, (c) matching comparison between the target EC8 elastic response spectrum $S_a^*(T_i, \zeta)$ and the generated accelerogram's response spectrum $S_a(T_i, \zeta)$, (d) acceleration time-history. The target PGA is denoted with the red dashed line.
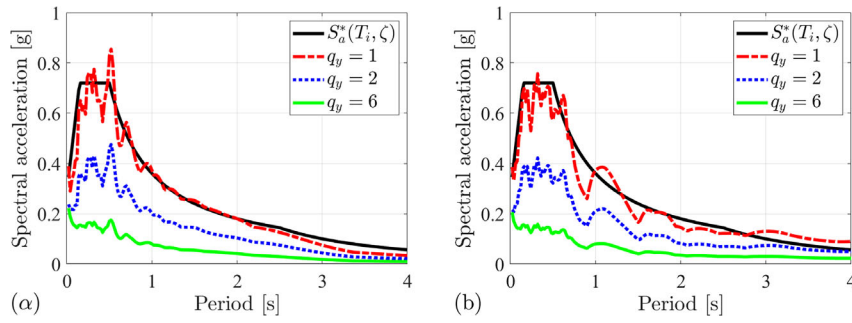
FIGURE 16 │ (a) Target elastic response spectrum $S_a^*(T_i, \zeta)$ and constant strength spectra for $q_y = 1$, $q_y = 2$, and $q_y = 6$ of the generated ground motion with the proposed methodology shown in Figure 8, (b) Target elastic response spectrum $S_a^*(T_i, \zeta)$ and constant strength spectra for $q_y = 1$, $q_y = 2$, $q_y = 6$ of the generated ground motion with the Cacciola [14] model shown in Figure 15.
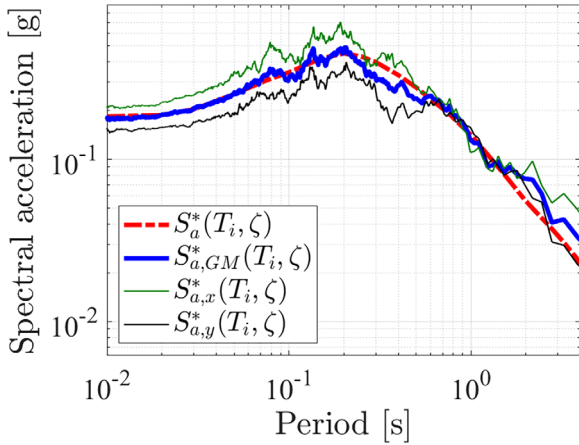

FIGURE 17 │ The two generated orthogonal target spectra $S_{a,x}^*(T_i, \zeta)$ and $S_{a,y}^*(T_i, \zeta)$, along with their geometric mean spectrum $S_{a,GM}^*(T_i, \zeta)$ as well as the target $S_a^*(T_i, \zeta)$.

Finally, Figure 16 shows the non-linear response spectra of the generated ground motions for the case of constant strength. Figure 16a shows the constant strength spectra for $q_y = 1$, $q_y = 2$, and $q_y = 6$ of the generated ground motion of Figure 8, and Figure 16b shows the same spectra obtained for the generated ground motion with the Cacciola [14] model shown in Figure 15. In both cases, the elastic target spectrum is also shown. It is observed that for $q_y = 1$ the resulting spectra are very close to the target, as expected.

7.2 │ Second Example: Generation of Bidirectional Ground Motion Components

The target geometric mean spectrum is obtained using the BSSA 14 [58] GMM. The considered seismic hazard scenario corresponds to moment magnitude $M_w = 6.5$, Joyner–Boore distance $R_{JB} = 10$ km, and $\varepsilon = 1$. The fault type is normal, and the rest of the parameters are kept as defined in the previous example. The two orthogonal target spectra $S_{a,x}^*(T_i, \zeta)$ and $S_{a,y}^*(T_i, \zeta)$ are produced following Equations (25)–(28). The model constraints are that the MSE of the geometric mean of the accepted ground motion pair with the target spectrum should be less than 5%, and the weights of Equation (28) are set equal to $w_1 = 1$, $w_2 = 0.07$, and $w_3 = 0.07$. The produced spectra are shown in Figure 17,

along with their geometric mean spectrum $S_{a,GM}^*(T_i, \zeta)$ as well as the target $S_a^*(T_i, \zeta)$.[5] The MSE between $S_a^*(T_i, \zeta)$ and $S_{a,GM}^*(T_i, \zeta)$ is $e = 2\%$, and $\rho_{S_{a,x}(T), S_{a,y}(T)} = 0.96 > 0.95$.

Once the $S_{a,x}^*(T_i, \zeta)$ and $S_{a,y}^*(T_i, \zeta)$ values are obtained, the two horizontal components are generated following the procedure presented in Section 4, for every component, individually. The produced bidirectional artificial acceleration time-histories $a_x(t)$ and $a_y(t)$ are shown in Figures 18 and 19. A final check is performed in order to ensure that the temporal correlation coefficient $\rho_{a_x(t), a_y(t)}$ is less than 0.30. This criterion is usually met; if it is not fulfilled, the procedure is repeated and a new pair of bidirectional ground motions is obtained. Finally, Figure 20 shows the comparison of the geometric mean response spectrum $S_{a,GM}(T_i, \zeta)$ of the produced ground motions with the target spectrum $S_a^*(T_i, \zeta)$. The MSE between $S_a^*(T_i, \zeta)$ and $S_{a,GM}(T_i, \zeta)$ is $e = 3\%$.

As it is observed, the generated bidirectional ground motions fulfill the criteria of the geometric mean spectra matching, as well as the temporal correlation criterion. It is also noted that the strong motion durations of the motions are $t_{x,5-95} = 8$ s and $t_{y,5-95} = 10$ s, thus they are representative of the same event. Moreover, even though one seed record was used, the two components exhibit different characteristics, as shown in Figures 18 and 19. Therefore, the proposed methodology is quite efficient for the generation of bidirectional ground motion components.

8 │ Conclusions

A novel and computationally efficient site- and spectrum-based stochastic methodology for the generation of bidirectional fully nonstationary artificial accelerograms is proposed. The model combines well-established tools such as the SRM with the CWT method and works proportionally to the evolutionary spectrum methods that modify a stationary signal in order to achieve full nonstationarity. Specifically, the amplitude and frequency non-stationarity is modeled after a time-frequency modulating function extracted from a past-recorded accelerogram from the site of interest; thus the simulated ground motions exhibit realistic nonstationary characteristics. Spectrum compatibility is ensured by a stationary and target spectrum-compatible stochastic process generated with the SRM. Therefore, the methodology accounts for an indirect modeling of the power spectrum.
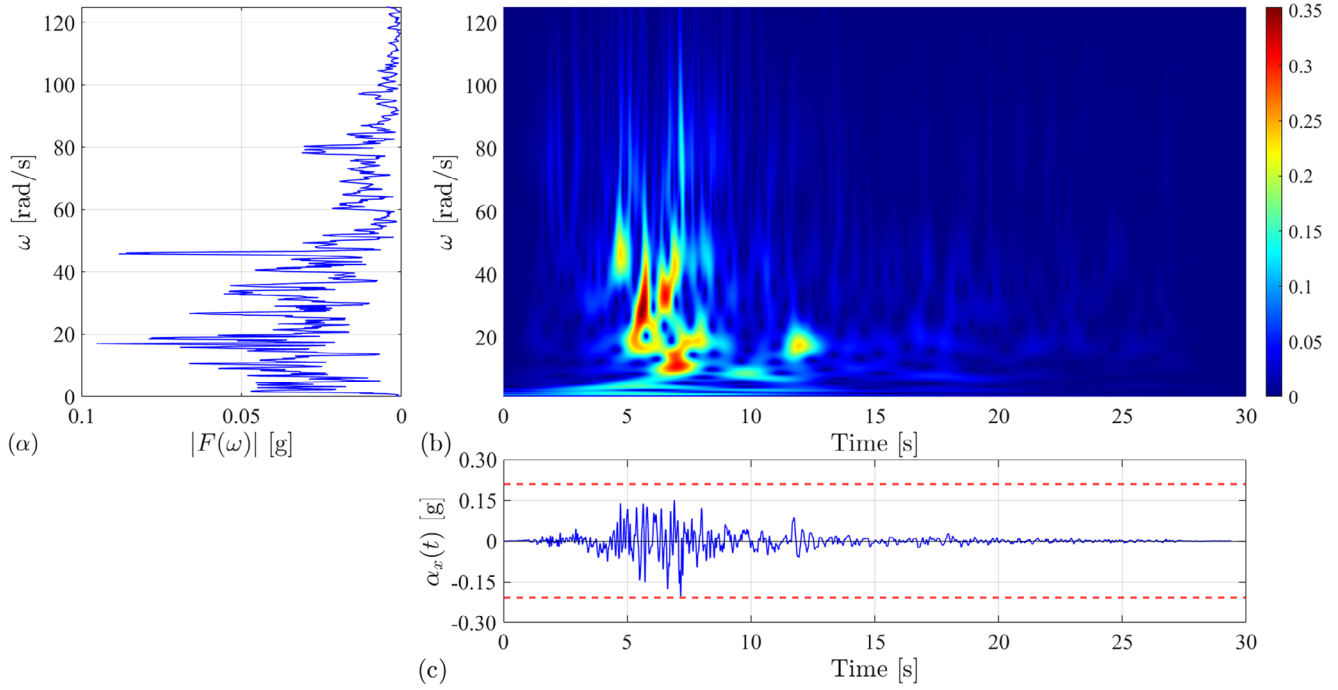
FIGURE 18 | The generated $a_x(t)$ component. (a) $|F(\omega)|$ plot, (b) $\left|T_\psi[a_x](\omega, b)\right|$ plot, (c) acceleration time-history. The target PGA is denoted with the red dashed line.
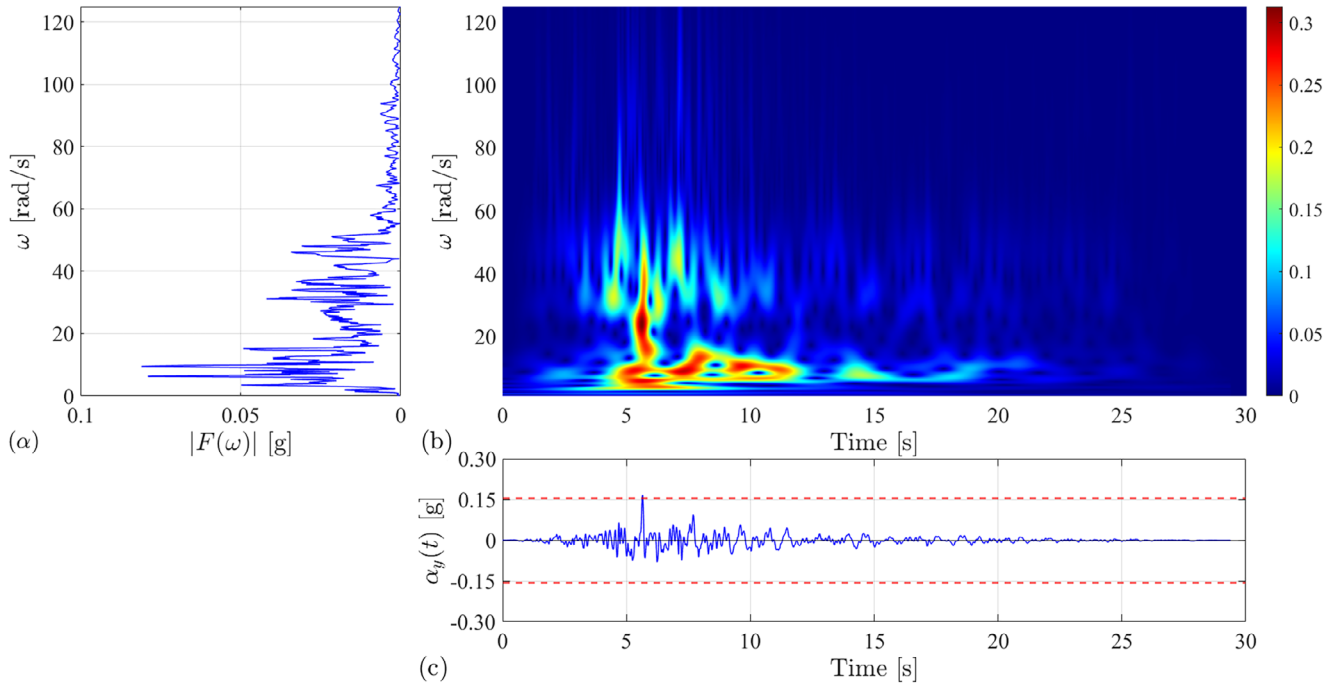

FIGURE 19 | The generated $a_y(t)$ component. (a) $|F(\omega)|$ plot, (b) $\left|T_\psi[a_y](\omega, b)\right|$ plot, (c) acceleration time-history. The target PGA is denoted with the red dashed line.

The CWT method adopted using the $L^2(\mathbb{R})$ normalization offers a robust representation of the seismic signal's energy evolution in time and a high time-scale (thus time-frequency) resolution. Therefore, fully nonstationary signals are directly modeled through a nonseparable process in the time-frequency domain, rather than being treated separately for the amplitude and for the frequency modulation at each respective domain, as for example

in [26]. It is noted that the $L^1(\mathbb{R})$ normalization is not suitable for the proposed methodology.

Regarding the choice of the seed records, they are expected to be obtained from past seismic activity from the site of interest, or from a site that has similar characteristics. It is noted that, during the analyses of the proposed methodology, it was observed
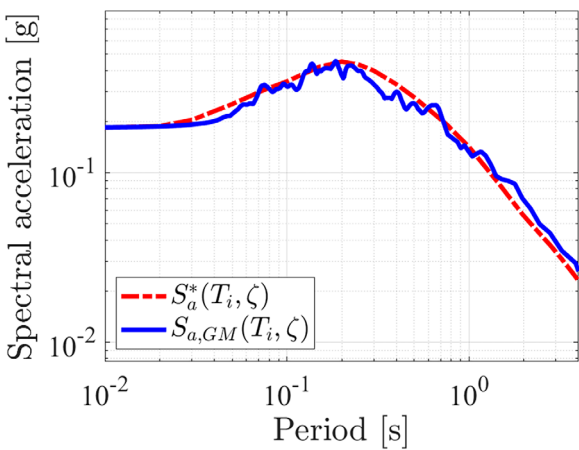
FIGURE 20 | Comparison of the geometric mean response spectrum $S_{a,GM}(T_i, \zeta)$ of the produced ground motions with the target spectrum $S_a^*(T_i, \zeta)$.

that if the selected record contains a pulse, that feature would be propagated to the generated ground motions. The proposed methodology provides with any required number of seismic accelerograms whose temporal and spectral modulation is consistent with a site of interest. Moreover, the generated signals represent entirely new ground motions, rather than modified versions of the seed record. It is also noted that the proposed methodology is straightforward, requiring only a seed record and a target spectrum as inputs, thus it can be applied in the engineering practice.

The choice of the mother wavelet affects the results of the proposed methodology. Specifically, the mother wavelets should be analytic. Furthermore, in order to achieve nonstationarity as well as good spectrum matching, it is recommended to use mother wavelets with an increased number of oscillation cycles and with a center frequency ω_ψ^* close to the dominant frequency of the stationary signal.

During postprocessing part, the Fourier transform was chosen over using the wavelet coefficients, since: (i) the corrective iterations are not always necessary, for example, as in the case of a smooth target spectrum, (ii) depending on the mother wavelet choice, the reconstruction of the signal using the inverse CWT might not be perfect. This would add extra error within an iterative procedure where the signal is repeatedly transformed from the time domain to the time-frequency domain and back. (iii) When an increased number of corrective iterations is desired (e.g., for very tight spectral matching), repeatedly converting the signal from the time domain to the time-frequency domain is computationally demanding.

The proposed model can also generate pairs of bidirectional horizontal components, by probabilistically producing two appropriate orthogonal target spectra whose geometric mean matches a target median spectrum obtained from a GMM. These spectra take into account the correlation structure of spectral acceleration pairs in orthogonal directions at different periods from empirical models, therefore, only a single-component ground motion is required as a seed record. The approach is a straightforward procedure that can be tailored to any seismic hazard scenario

represented by a target acceleration spectrum, for example, a CMS, a GMM, or a design code spectrum. Moreover, the proposed methodology is not limited to the presented ground motion generation methodology, but it can be applied to other site and spectrum-based models.

Some possible alternatives and extensions of the proposed methodology are mentioned. An appropriate time-frequency modulating function, modeled by a mathematical equation can be used instead of a seed record. However, this would result in several modifications to the proposed procedure, and it would require assumptions for various ground motion parameters like the strong motion duration and the energy content of the signal to be generated. These requirements could be fulfilled either using empirical GMMs as in [16] or by parameterizing an online database of recorded motions. The proposed methodology can also be used to generate suites of fully nonstationary artificial accelerograms matching a target mean spectrum and variability, by employing the procedure presented in [16]. In this methodology, multiple target response spectra are produced from a random vector that follows the normal distribution and is statistically defined by the target spectral mean and variability. For each of these spectra, a corresponding spectrum-compatible artificial accelerogram can be generated, following the proposed wavelet-based procedure and using randomly sampled appropriate seed records.

Finally, it is noted that the proposed methodology is computationally efficient, as both the generation of single components and bidirectional components is a matter of seconds. Moreover, its implementation is identified as a straightforward task in MATLAB [56] environment. Therefore, the proposed model aims to offer a practical tool for engineering applications in a consistent and code-compliant manner, as well as for stochastic dynamics problems.

Data Availability Statement

The data that support the findings of this study are available from the corresponding author upon reasonable request.

Endnotes

[1] $\int_{-\infty}^{+\infty} |\psi(t)|^2 \, dt < \infty$.

[2] It is noted that the asterisk as superscript denotes the parameters that serve as target values.

[3] $e = \frac{\sum_{i=1}^{N} \left| X_i - X_i' \right|^2}{N}$, where X_i' is the target output value and X_i is the actual output value.

[4] A Husid plot is the plot of the normalized accumulation of Arias intensity with time [57].

[5] The median of data that follows a lognormal distribution is approximately equal to the mean of the logarithms. Thus, the comparisons on

Earthquake Engineering & Structural Dynamics, 2025

the following are performed between the median spectral values instead of logarithmic.

References

1. M. Fragiadakis and N. D. Lagaros, "An Overview to Structural Seismic Design Optimisation Frameworks," *Computers & Structures* 89, no. 11 (2011): 1155–1165.

2. C. Song and R. Kawai, "Monte Carlo and Variance Reduction Methods for Structural Reliability Analysis: A Comprehensive Review," *Probabilistic Engineering Mechanics* 73 (2023): 103479.

3. I. P. Mitseas, I. A. Kougioumtzoglou, M. Beer, E. Patelli, and J. E. Mottershead, "Robust Design Optimization of Structural Systems Under Evolutionary Stochastic Seismic Excitation," in *Vulnerability, Uncertainty, and Risk: Quantification, Mitigation, and Management* (Reston, Virginia: ASCE, 2014), https://doi.org/10.1061/9780784413609.022.

4. I. A. Kougioumtzoglou, P. Ni, I. P. Mitseas, V. C. Fragkoulis, and M. Beer, "An Approximate Stochastic Dynamics Approach for Design Spectrum Based Response Analysis of Nonlinear Structural Systems With Fractional Derivative Elements," *International Journal of Non-Linear Mechanics* 146 (2022): 104178.

5. D. J. Jerez, V. C. Fragkoulis, P. Ni, et al., "Operator Norm-Based Determination of Failure Probability of Nonlinear Oscillators With Fractional Derivative Elements Subject to Imprecise Stationary Gaussian Loads," *Mechanical Systems and Signal Processing* 208 (2024): 111043.

6. P. Ni, I. P. Mitseas, V. C. Fragkoulis, and M. Beer, "Spectral Incremental Dynamic Methodology for Nonlinear Structural Systems Endowed With Fractional Derivative Elements Subjected to Fully non-Stationary Stochastic Excitation," *Structural Safety* 111 (2024): 102525.

7. F. Scozzese, E. Tubaldi, and A. Dall'Asta, "Assessment of the Effectiveness of Multiple-Stripe Analysis by Using a Stochastic Earthquake Input Model," *Bulletin of Earthquake Engineering* 18, no. 7 (2020): 3167–3203.

8. G. Abbiati, M. Broccardo, I. Abdallah, S. Marelli, and F. Paolacci, "Seismic Fragility Analysis Based on Artificial Ground Motions and Surrogate Modeling of Validated Structural Simulators," *Earthquake Engineering & Structural Dynamics* 50 (2021): 2314–2333.

9. A. Zacharenaki, M. Fragiadakis, D. Assimaki, and M. Papadrakakis, "Bias Assessment in Incremental Dynamic Analysis due to Record Scaling," *Soil Dynamics and Earthquake Engineering* 67 (2014): 158–168.

10. M. Grigoriou, "Do Seismic Intensity Measures (IMs) Measure up?," *Probabilistic Engineering Mechanics* 46 (2016): 80–93.

11. D. M. Boore, "Simulation of Ground Motion Using the Stochastic Method," *Pure and Applied Geophysics* 160 (2003): 635–676.

12. D. M. Boore, "Comparing Stochastic Point-Source and Finite-Source Ground-Motion Simulations: SMSIM and EXSIM," *Bulletin of the Seismological Society of America* 99 (2009): 3202–3216.

13. S. Rezaeian and A. Der Kiureghian, "A Stochastic Ground Motion Model With Separable Temporal and Spectral Nonstationarities," *Earthquake Engineering & Structural Dynamics* 37, no. 13 (2008): 1565–1584.

14. P. Cacciola, "A Stochastic Approach for Generating Spectrum Compatible Fully Nonstationary Earthquakes," *Computers & Structures* 88 (2010): 889–901.

15. R. Sharbati, F. Khoshnoudian, H. Ramazi, and H. Amindavar, "Stochastic Modeling and Simulation of Ground Motions Using Complex Discrete Wavelet Transform and Gaussian Mixture Model," *Soil Dynamics and Earthquake Engineering* 114 (2018): 267–280.

16. H. Yanni, M. Fragiadakis, and I. P. Mitseas, "Probabilistic Generation of Hazard-Consistent Suites of Fully non-Stationary Seismic Records," *Earthquake Engineering & Structural Dynamics* 53, no. 10 (2024): 3140–3164.

17. E. H. Vanmarcke and D. A. Gasparini, "Simulated Earthquake Ground Motions," in *Proceedings of the 4th International Conference on Structural Mechanics in Reactor Technology (SMiRT 4)* (San Francisco, USA: IASMiRT, 1977).

18. P. Spanos and L. V. Loli, "A Statistical Approach to Generation of Design Spectrum Compatible Earthquake Time Histories," *International Journal of Soil Dynamics and Earthquake Engineering* 4 (1985): 2–8.

19. S. Mukherjee and V. K. Gupta, "Wavelet-Based Generation of Spectrum-Compatible Time-Histories," *Soil Dynamics and Earthquake Engineering* 22, no. 9 (2002): 799–804.

20. S. H. Ni, W. C. Xie, and M. D. Pandey, "Generation of Spectrum-Compatible Earthquake Ground Motions Considering Intrinsic Spectral Variability Using Hilbert-Huang Transform," *Structural Safety* 42 (2013): 45–53.

21. A. Giaralis and P. D. Spanos, "Wavelet-Based Response Spectrum Compatible Synthesis of Accelerograms-Eurocode Application (EC8)," *Soil Dynamics and Earthquake Engineering* 29 (2009): 219–235.

22. M. Baglio, A. Cardoni, G. P. Cimellaro, and N. Abrahamson, "Generating Ground Motions Using the Fourier Amplitude Spectrum," *Earthquake Engineering & Structural Dynamics* 52, no. 15 (2023): 4884–4899.

23. Y. Yamamoto and J. W. Baker, "Stochastic Model for Earthquake Ground Motion Using Wavelet Packets," *Bulletin of the Seismological Society of America* 103 (2013): 3044–3056.

24. M. Dabaghi and A. Der Kiureghian, "Stochastic Model for Simulation of Near-Fault Ground Motions," *Earthquake Engineering & Structural Dynamics* 46, no. 6 (2017): 963–984.

25. C. Vlachos, K. G. Papakonstantinou, and G. Deodatis, "Predictive Model for Site Specific Simulation of Ground Motions Based on Earthquake Scenarios," *Earthquake Engineering & Structural Dynamics* 47, no. 1 (2018): 195–218.

26. F. Sabetta, A. Pugliese, G. Fiorentino, G. Lanzano, and L. Luzi, "Simulation of non-Stationary Stochastic Ground Motions Based on Recent Italian Earthquakes," *Bulletin of Earthquake Engineering* 19, no. 9 (2021): 3287–3315.

27. C. Jin and J. Hu, "A New Ground-Motion Simulation Procedure Based on Feature Extraction Matching Multiple Intensity Measures," *Soil Dynamics and Earthquake Engineering* 168 (2023): 107856.

28. Pacific Earthquake Engineering Research Center (PEER) Ground Motion Database, *NGA-West2 – Shallow Crustal Earthquakes in Active Tectonic Regimes*, https://ngawest2.berkeley.edu (Last accessed: July 2024).

29. S. Rezaeian and A. DerKiureghian, "Simulation of Orthogonal Horizontal Ground Motion Components for Specified Earthquake and Site Characteristics," *Earthquake Engineering & Structural Dynamics* 41, no. 2 (2012): 335–353.

30. D. Huang and Z. Wang, "Wavelet-Based Stochastic Model for Jointly Simulating Three-Component Ground Motions," *Bulletin of the Seismological Society of America* 112, no. 3 (2022): 1483–1501.

31. S. Liao and A. Zerva, "Physically Compliant, Conditionally Simulated Spatially Variable Seismic Ground Motions for Performance-Based Design," *Earthquake Engineering & Structural Dynamics* 35, no. 7 (2006): 891–919.

32. M. Shinozuka and G. Deodatis, "Simulation of Stochastic Processes by Spectral Representation," *Applied Mechanics Reviews* 44 (1991): 191–204.

33. M. B. Priestley, *Spectral Analysis and Time Series, Two-Volume Set*, 1st ed. (London, UK: Academic Press, 1982).

34. E. H. Vanmarcke, "Structural Response to Earthquakes," *Developments in Geotechnical Engineering*, Vol. 15 (Amsterdam, The Netherlands: Elsevier, 1976).

35. A. Giaralis and P. D. Spanos, "Derivation of Response Spectrum Compatible Non-Stationary Stochastic Processes Relying on Monte Carlo-Based Peak Factor Estimation," *Earthquakes and Structures* 3 (2012): 581–609.

36. P. D. Spanos, A. Giaralis, and L. Jie, "Synthesis of Accelerograms Compatible With the Chinese GB 50011-2001 Design Spectrum via Harmonic Wavelets: Artificial and Historic Records," *Earthquake Engineering and Engineering Vibration* 8 (2009): 189–206.

37. L. A. Montejo and L. E. Suarez, "An Improved CWT-Based Algorithm for the Generation of Spectrum-Compatible Records," *International Journal of Advanced Structural* 5, no. 1 (2013): 26.

38. P. D. Spanos, A. Giaralis, and N. P. Politis, "Time-Frequency Representation of Earthquake Accelerograms and Inelastic Structural Response Records Using the Adaptive Chirplet Decomposition and Empirical Mode Decomposition," *Soil Dynamics and Earthquake Engineering* 27, no. 7 (2007): 675–689.

39. P. D. Spanos, A. Giaralis, N. P. Politis, and J. M. Roesset, "Numerical Treatment of Seismic Accelerograms and of Inelastic Seismic Structural Responses Using Harmonic Wavelets," *Computer-Aided Civil and Infrastructure Engineering* 22, no. 4 (2007): 254–264.

40. ASCE/SEI 7–22, *Minimum Design Loads and Associated Criteria for Buildings and Other Structures* (Reston, VA, USA: American Society of Civil Engineers, 2021).

41. N. Jayaram, T. Lin, and J. Baker, "A Computationally Efficient Ground-Motion Selection Algorithm for Matching a Target Response Spectrum Mean and Variance," *Earthquake Spectra* 27 (2011): 797–815.

42. J. W. Baker and N. Jayaram, "Correlation of Spectral Acceleration Values from NGA Ground Motion Models," *Earthquake Spectra* 24 (2008): 299–317.

43. H. Yanni, *Wavelet-Based Stochastic Model for the Generation of Fully Non-Stationary Bidirectional Seismic Accelerograms* (Athens, Greece: National Technical University of Athens, 2024), [GitHub Repositories]. https://github.com/HeraYanni/WaveletGenArtifAccel, and https://github.com/HeraYanni/BidirectionalArtifAccel.

44. P. Cacciola, P. Colajanni, and G. Muscolino, "Combination of Modal Responses Consistent with Seismic Input Representation," *Journal of Structural Engineering* 130 (2004): 47–55.

45. E. H. Vanmarcke, "Properties of Spectral Moments With Applications to Random Vibration," *Journal of the Engineering Mechanics Division* 98 (1972): 425–446.

46. A. D. Kiureghian, "Structural Response to Stationary Excitation," *Journal of the Engineering Mechanics Division* 106 (1980): 1195–1213.

47. C. K. Chui, *An Introduction to Wavelets, Wavelet Analysis and Its Applications*, Vol. 1 (Boston, MA: Academic Press, 1992).

48. S. Mallat, *A Wavelet Tour of Signal Processing, The Sparse Way*, 3rd ed. (Burlington, MA: Academic Press, 2009).

49. P. Argoul and M. Fragiadakis, "Application of the Wavelet Transform Inverse Analysis for Modal Identification and Damage Detection," in *Proceedings of the 9th International Conference on Computational Methods in Structural Dynamics and Earthquake Engineering (COMPDYN 2023)* (Athens, Greece: National Technical University of Athens, 2023).

50. P. D. Spanos and G. Failla, "Evolutionary Spectra Estimation Using Wavelets," *Journal of Engineering Mechanics* 130 (2004): 952–960.

51. C. Torrence and G. P. Compo, "A Practical Guide to Wavelet Analysis," *Bulletin of the American Meteorological Society* 79 (1998): 61–78.

52. J. M. Lilly and S. C. Olhede, "Generalized Morse Wavelets as a Superfamily of Analytic Wavelets," *IEEE Transactions on Signal Processing* 60, no. 11 (2012): 6036–6041.

53. National Institute of Standards and Technology, "Selecting and Scaling Earthquake Ground Motions for Performing Response History Analyses," Rep. No. NIST GCR 11-917-15 (2011).

54. N. Jayaram and J. Baker, "Statistical Tests of the Joint Distribution of Spectral Acceleration Values," *Bulletin of the Seismological Society of America* 98 (2008): 2231–2243.

55. Eurocode 8 (EN1998-1), *Design of Structures for Earthquake Resistance—Part I: General Rules, Seismic Actions and Rules for Buildings* (Brussels, Belgium: European Committee for Standardization, 2004).

56. MathWorks, *MATLABversion 2024a* (2024), [Computer Software] https://www.mathworks.com/products/matlab.html.

57. S. L. Kramer, *Geotechnical Earthquake Engineering*, Prentice-Hall International Series in Civil Engineering and Engineering Mechanics (Upper Saddle River, New Jersey, USA: Prentice-Hall, 1996).

58. D. M. Boore, J. P. Stewart, E. Seyhan, and G. M. Atkinson, "NGA-West2 Equations for Predicting PGA, PGV, and 5% Damped PSA for Shallow Crustal Earthquakes," *Earthquake Spectra* 30 (2014): 1057–1085.